PNNL-31954

Light Water Reactor Sustainability Program

Evaluation of Oxygen Consumption as a Sensitive Measure of Electrical Cable Polymer Insulation Degradation

September 2021

U.S. Department of Energy

Office of Nuclear Energy

PNNL-31954

Light Water Reactor Sustainability Program
Milestone M3LW-20OR0404017

Evaluation of Oxygen Consumption as a Sensitive Measure of Electrical Cable Polymer Insulation Degradation

Leonard S. Fifield, Yelin Ni, Aishwarya Sriraman, Witold Fuchs, Donghui Li, Madhusudhan R. Pallaka, Mychal P. Spencer, Katarzyna Grubel, Jonathan D. Egbert, and Andy Zwoster

September 2021

Prepared for the
U.S. Department of Energy
Office of Nuclear Energy

SUMMARY

Polymers used as dielectric materials in nuclear grade electrical cables, such as cross-linked polyethylene (XLPE) and ethylene-propylene rubber (EPR), are long-lived and durable. Estimating the decades-long service life of polymers experimentally in a feasible timeframe of weeks or months requires greatly accelerated aging in the laboratory at drastically elevated temperatures and/or gamma dose rates. Many limitations of accelerated aging, such as diffusion limited oxidation and dose rate effects, have been identified that can make accurate lifetime prediction at service conditions challenging. This can be due to differences in degradation mechanisms between rapid and extended aging or to the presence of induction periods during which early aging is undetectable using common metrics of polymer insulation characterization, such as tensile elongation at break.

Conceptually, an ideal measure of aging would track clearly and predictably with material changes throughout the lifecycle of the evolving material state from early aging through end of useful life. With such a metric, accelerated aging could be performed at much milder conditions, conditions closer to those found in long term service, and end of life calculated from the early data. Oxygen consumption has previously been proposed as a sensitive measure of polymer insulation oxidation that might meet such desirable characteristics.

In this work, nuclear cable insulation samples of the two most common types, XLPE and EPR, from two of the most sourced manufacturers, RSCC Wire & Cable Inc. and The Okonite Company, were subjected to gamma irradiation at dose rates of 100, 200, and 300 Gy/hr for up to 42 days at 26°C. The aged samples were used to evaluate oxygen consumption as a sensitive measure of aging for these materials and these conditions. For comparison and validation, the aged samples were also characterized using the more conventional tests of mass change, density, carbonyl index, and yellowness index.

Compared to the conventional tests, oxygen consumption was found to be a particularly sensitive metric to measure the degradation of polymeric cable insulation exposed to radiation. For both materials, oxygen consumption during irradiation was found to track linearly with applied dose—oxygen consumption rate was constant with time. Oxygen consumption rate was compared to time-temperature-superposition methods for Arrhenius activation energy calculation using literature data and found to be a useful and viable alternative for lifetime prediction. Both mass change and carbonyl index were clearly proportional to exposure dose. Yellowness index, a surface sensitive measure, was observed to increase linearly with dose at low exposure levels before plateauing, while density was not observed to change under the conditions explored.

The techniques developed in this work are anticipated to be valuable in the estimation of insulation aging rates under mild conditions approaching service conditions. Direct comparison of useful life prediction by oxygen consumption with prediction via Arrhenius methodology for thermal aging and existing methods for radiation and combined thermal/radiation aging would serve to further validate this promising approach and refine our understanding of material-specific aging rates.

ACKNOWLEDGEMENTS

This work was sponsored by the U.S. Department of Energy (DOE) Office of Nuclear Energy (NE) Light Water Reactor Sustainability (LWRS) Program Materials Research Pathway. The authors extend their appreciation to Pathway Lead Dr. Thomas Rosseel for LWRS programmatic support. Support for gamma irradiation at Sandia National Laboratories (SNL) of the samples described in this report was provided through the Nuclear Science User Facilities (NSUF) program: FY 2020 Consolidated Innovative Nuclear Research Funding Opportunity Announcement (FOA), DE-FOA-0002128, CFA-20-19145, "Improving Lifetime Prediction of Electrical Cables in Containment" award. SNL staff Donald J. Hanson and Maryla Wasiolek are gratefully acknowledged for their assistance with the irradiation. Preparation, testing and analysis of samples was performed at the Pacific Northwest National Laboratory (PNNL). PNNL is operated by Battelle for the U.S. Department of Energy under contract DE-AC05-76RL01830.

CONTENTS

FIGURES

TABLES

ACRONYMS AND ABBREVIATIONS

BAS	basic auto-oxidation scheme
CI	carbonyl index
CIE	Commission on Illumination
CSPE	chlorosulfonated polyethylene
ΔE^*_{ab}	total color difference
E_a	activation energy
EAB	elongation at break
EPR	ethylene-propylene rubber
EMDA	Expanded Materials Degradation Assessment
EPDM	ethylene-propylene-diene elastomer
EPRI	Electric Power Research Institute
ETFE	ethylene-tetrafluoroethylene
FTIR	Fourier-transform infrared spectroscopy
IEC	International Electrotechnical Commission
IEEE	Institute of Electrical and Electronics Engineers
IPA	isopropanol (2-propanol)
IPAM	Indenter Polymer Aging Monitor
ISO	International Standards Organization
LWRS	Light Water Reactor Sustainability
NPP	nuclear power plant
NIH	National Institute of Health
PE	Polyethylene
PNNL	Pacific Northwest National Laboratory
PVC	polyvinyl chloride
ROI	region of interest
SLR	subsequent license renewal
SR	silicone rubber
sRGB	standard red-green-blue
XLPE	cross-linked polyethylene
ϕ	oxygen consumption rate

1. INTRODUCTION

Prediction of the service life of electrical cable insulation used in nuclear power plants (NPPs) is based on observable time-dependent material properties, see Figure 1. In practice, polymeric insulation samples are challenged at accelerated aging conditions in the lab, t_2 in Equation (1), specifically at temperatures (T_2) and/or gamma dose rates (I_2) higher than their NPP service conditions (T_1, I_1) to gain insight into the degradation of their material properties. Times to selected endpoints measured at accelerated conditions are extrapolated to service conditions by shifting the curves on logarithmic time axes (or equivalently, stretching the curves on linear time axes) where the form factor a is given by Equation (1). Assumptions behind this shifting process include that (1) the aging process is isodosic, that is, independent of dose rate, (2) it has an Arrhenius temperature dependence, (3) the dose rate and temperature dependencies are additive, and (4) model parameters such as Arrhenius activation energy (E_a) are the same in the target aging condition (Celina, Clough and Gillen, 1998; Martin *et al.*, 2008; Celina, 2013).

$$a = \frac{t_1}{t_2} = \frac{I_2}{I_1} \times \exp\left(\frac{E_a}{R}\left(\frac{1}{T_1} - \frac{1}{T_2}\right)\right), \quad R = \text{universal gas constant} \tag{1}$$

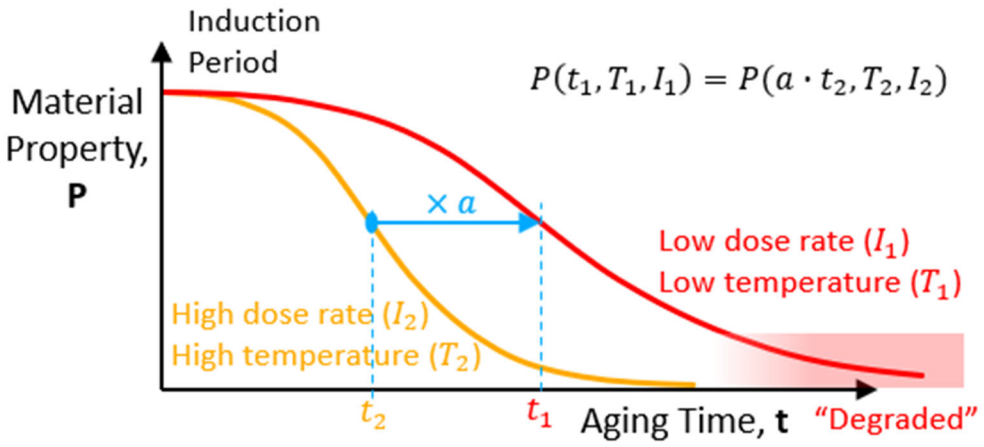

Figure 1. Predicting long-term behavior (red curve) from tested properties at accelerated aging conditions (yellow curve) by stretching along the time axis.

Many scenarios have been identified where the above assumptions are violated, namely, in the presence of phenomena including inverse temperature effects (Celina *et al.*, 1996), dose rate effects (Wise, Gillen and Clough, 1997), diffusion limited oxidation (Gillen and Clough, 1992; Audouin *et al.*, 1994; Wise, Gillen and Clough, 1997), synergistic effects (NUREG/CR-7153, 2014) and decrease in activation energy at lower temperatures (Celina, Clough and Gillen, 1998; Gillen, Celina and Bernstein, 2003; Celina, Gillen and Assink, 2005; Gillen, Bernstein and Celina, 2005). Even when these aging artefacts are avoided, determination of model constants from isotherms and/or iso-dose-rate curves requires months or years of aging time, several different test conditions, and many test samples. A potential strategy to circumvent these limitations is the use of sensitive measures of aging (SMA), which are analysis techniques that can detect material degradation at early stages of aging or under relatively mild conditions such as those experienced during cable service life. SMAs could, therefore, be used to predict material performance at conditions where traditional material lifetime prediction metrics (e.g., elongation at break or density) do not exhibit sufficient sensitivity to provide useful information (Gillen *et al.*, 2006). However, SMAs remain poorly explored in the literature and basic knowledge regarding which techniques are suitable as SMAs and how they compare to more traditional test methods remains scarce.

An excellent candidate for a SMA is oxygen consumption (OC), as measured by gas chromatography (GC) (Assink *et al.*, 2005). Oxygen consumption has been reported to be quantifiable and exhibit linear evolution with time at early stages of degradation, which are vital qualities of SMAs (Wise, Gillen and Clough, 1995; Gillen, Celina and Keenan, 2000; Gillen, Celina and Bernstein, 2003; Celina, Dayile and Quintana, 2013). However, it is not clear if or when OC will deviate from linear behavior (i.e., when the OC rate will change). A measurable change in OC rate could indicate that a different degradation mechanism begins to dominate the overall kinetics and could confound analysis attempts (Craig *et al.*, 2005; François-Heude *et al.*, 2015; Wypych, 2020). In this work, OC was compared to traditional material performance metrics and evaluated as an SMA on the two most common cable insulation materials, crosslinked polyethylene (XLPE) and ethylene-propylene rubber (EPR). Furthermore, OC behavior of the selected cable insulation materials was evaluated for linearity to establish whether complicating factors are present and would preclude valuable analyses using this technique.

2. OXIDATIVE DEGRADATION

The rate of oxygen consumption in polymers has previously been investigated using a modified form of the basic autoxidation scheme (BAS) (Gillen, Wise and Clough, 1995). The BAS was initially proposed for oxidation of unsaturated fatty acids (Bolland and Gee, 1946) that exhibited behavior similar to the free autocatalytic radical depolymerization. A modified BAS has been proposed for polymer degradation where termination to antioxidants and disproportionation are considered in addition to chain scission and crosslinking considered in the original BAS (Gillen, Wise and Clough, 1995), see Figure 2.

$$\text{Polymer} \xrightarrow{I} \text{R}\cdot$$

$$\text{R}\cdot + \text{O}_2 \xrightarrow{k_2} \text{ROO}\cdot$$

$$\text{ROO}\cdot + \text{RH} \xrightarrow{k_3} \text{ROOH} + \text{R}\cdot$$

$$\text{ROOH} \xrightarrow{k_4} \text{RO}\cdot + \cdot\text{OH}$$

$$\text{ROO}\cdot, \text{R}\cdot, \text{RO}\cdot, \text{HO}\cdot \rightarrow \text{Products} \begin{cases} \text{scission} \\ \text{crosslinking} \\ \text{disproportion} \\ \text{antioxidant absorption} \end{cases}$$

Figure 2. Autoxidation mechanism for polyolefin.

Regardless of which pathway the termination reaction of Figure 2 follows, hydroperoxide (ROOH) is the intermediate product generated in the propagation step (François-Heude *et al.*, 2015; Da Cruz *et al.*, 2016). Homolysis of hydroperoxides generates more radicals, leading to autocatalysis. The acceleration is limited by radical concentration increases which cause a greater preponderance of termination reactions than initiation reactions or propagation reactions. Based on the scheme in Figure 2, the rate r of oxygen (O_2) consumption is given by Equation (2) (Audouin *et al.*, 1994; Gillen, Wise and Clough, 1995; Wise, Gillen and Clough, 1995), in which a and b are constants.

$$r_{O_2} = -\frac{d[O_2]}{dt} = \frac{a[O_2]}{1+b[O_2]} \tag{2}$$

In their service environment, electrical cable insulation is commonly exposed to ambient air containing oxygen. Assuming an unlimited source of oxygen (e.g., circulating air), the overall oxygen consumption reaction is zero order, and the OC rate is constant. On the other hand, if the concentration of oxygen surrounding the material approaches zero, oxygen consumption transitions to first order behavior and the rate becomes dependent on oxygen concentration, see Figure 3 (Verdu, 2012).

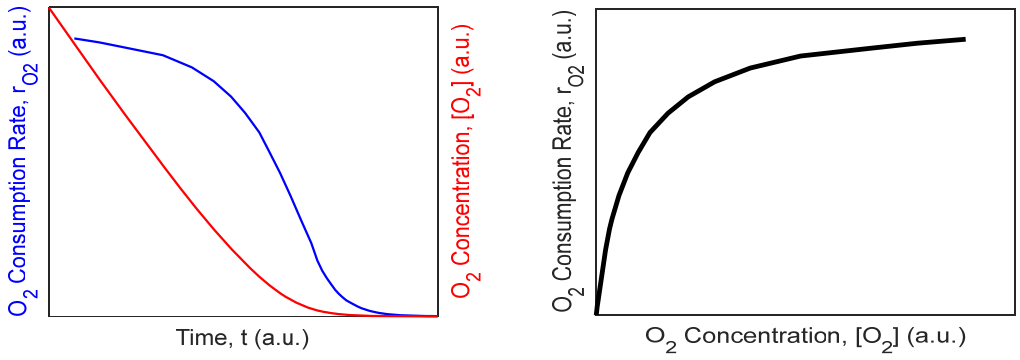

Figure 3. Oxygen consumption progression in autoxidation simulated by numerically solving Equation (2).

3. MATERIALS

The two materials investigated in this study, ethylene propylene rubber (EPR) and cross-linked polyethylene (XLPE), were chosen from among those that are typically employed in NPPs. As shown in Table 1, XLPE and EPR are the most abundantly used cable insulation materials inside nuclear containment. The test samples prepared for this work were extracted from commercial cables produced by two of the nine most common manufacturers of electrical cables for NPPs (Table 1 and Table 2). The as-received EPR-insulated cable in this report was harvested from the decommissioned Crystal River Unit 3 (Fifield *et al.*, 2016), where it was in service for 15 years (described in Table 2). The XLPE cable, on the other hand, was new and obtained directly from the manufacturer.

Table 1. Most common nuclear cable insulation material types in containment (left) and a sorted list of the most common insulations within NPPs (right). (Percent of units indicated are approximate values.)

Insulation	Percent of Units (%) (Subudhi, 1996)
XLPE	90
EPR/EPDM	75
SR	27
CSPE	24
ETFE	15
PVC	7
PE	3
Neoprene	3
Polyimide	3
Polyalkene	2

Manufacturer	Insulation	Number of Plants (Subudhi, 1996)
Rockbestos	Firewall III XLPE	61
Anaconda	EPR	35
Brand-Rex	XLPE	30
Okonite	EPR	26
Kerite	HTK	25
Rockbestos	Coaxial XLPE	24
Raychem	XLPE	23
Samuel Moore	EPR	19
BIW	Bostrad 7E EPR	19
Kerite	Flame Retardant EPR	13

XLPE = cross-linked polyethylene; EPDM = ethylene-propylene-diene elastomer; EPR = ethylene-propylene rubber; SR = silicone rubber; CSPE = chlorosulfonated polyethylene; ETFE = ethylene tetrafluoroethylene; PVC = polyvinyl chloride; PE = polyethylene; HTK = high-temperature Kerite.

Table 2. Nuclear grade instrumentation cables used in this report.

Sample ID	Manufacturer	Jacket Labeling	Jacket Material	Insulation Material	Service History
XLPE	RSCC Wire & Cable Inc.	2/C 16 AWG COPPER RSCC 600V FIREWALL III FRXLPE SHIELDED CSPE	CSPE	XLPE	New in 2015
EPR	The Okonite Company	OKONITE 4 3/C 14 AWG CU OKONITE FMR (EP)-CSPE 600V 18C 1998	CSPE	EPR	15 years

CSPE = chlorosulfonated polyethylene; EPR = ethylene-propylene rubber; XLPE = cross-linked polyethylene

3.1 Sample Extraction

Components of the low-voltage nuclear grade instrumentation cables of this report are shown in Figure 4. The test samples were prepared in three steps. First, insulated conductors were extracted from the electrical cables by carefully removing the external chlorosulfonated polyethylene (CSPE) jacket. Next, a wire stripping tool was used to score the insulation in 100 mm increments. Finally, the exposed conductor was fixed in place with a vice and the insulation was removed by gently pulling it from over the conductor (approximately 10% of the material was lost during this process). The extracted insulation samples were 100 mm in length. The tubular cross-sections of the insulation samples for XLPE and EPR were measured to be 5.06 mm^2 (2.81 mm outer diameter) and 12.17 mm^2 (4.32 mm outer diameter), respectively.

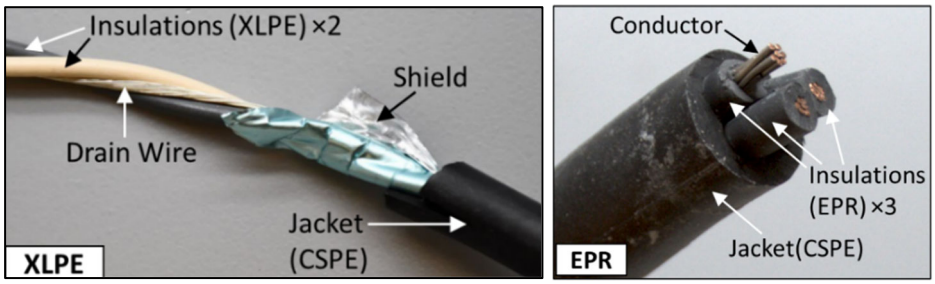

Figure 4. Exposed components of the evaluated (left) XLPE and (right) EPR electrical cables.

The material types of the extracted insulation were confirmed by comparing their Fourier-transform infrared (FTIR) absorbance spectra to data found in the literature (Grebowicz, Lau and Wunderlich, 1984; Nielsen, Batchelder and Pyrz, 2002). The spectra of the as-received insulation samples are shown in Figure 5, while the characteristic absorbance peaks for different functional groups are shown in Table 3. Both XLPE and EPR have a large fraction of methylene (-CH_2-) groups, which serves as a useful indicator for identifying these polymers. For example, both XLPE and EPR show sharp peaks at 2914 and 2847 cm^{-1}, which is attributed to -CH_2- vibrations. It was also noted that this EPR material has a weak carbonyl peak at 1601 cm^{-1} likely because of oxidation that may have occurred during its 15-year service history.

Table 3. Assignment of FTIR peaks detected on as-received XLPE and EPR samples.

Wavenumber (cm^{-1})	**Assignment**
2914	Asymmetric CH_2 stretching
2847	Symmetric CH_2 stretching
1601	C=O stretching
1462	CH_2 scissoring
1350	CH_2 wagging
1029	C-O stretching
801	C-C stretching
729	CH_2 rocking

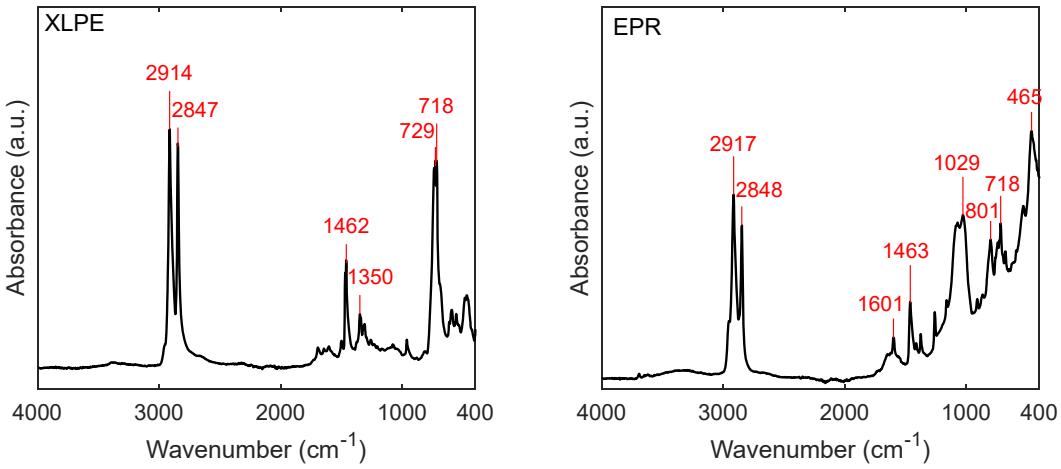

Figure 5. FTIR absorbance spectra for the as-received (left) XLPE and (right) EPR samples.

3.2 Sample Preparation

Test sample preparation was carried out prior to radiation aging. The insulation samples were sealed in 5-inch-long stainless-steel tubular vessels with 1-inch outer diameter. The vessels were assembled using Swagelok components as shown in Figure 6. For each vessel, 3 insulation samples constituting a total of approximately 3 g of polymer were placed inside. The tubes were capped on one end and connected to a rupture disk with a pressure relief threshold of 1900 psig on the other end to avoid any opportunity of over-pressurization. The rupture disk was then attached to a ball valve. The oxidative environment for the samples was selected to be purified air containing no hydrocarbons (Zero Air, Oxarc). Table 4 gives the fraction of gas components in the purified air as measured by gas chromatography, see Section 4.1. The volume of gas inside the assembled vessel was measured by the pressure-volume-temperature (PVT) method and is shown in Table 5.

Table 4. Percentage fraction of gas components in the zero or purified air.

Component	Hydrogen	Oxygen	Nitrogen	Methane	Carbon Monoxide	Carbon Dioxide	Other
Fraction (%)	0.0	21.2 ± 0.2	71.5 ± 0.2	0.0	0.0	0.0	7.30 ± 0.3

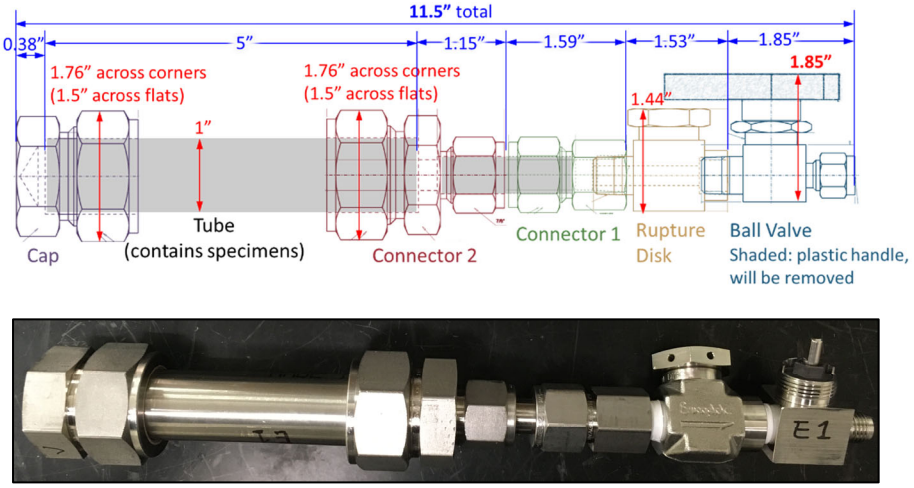

Figure 6. (Top) schematic and (bottom) digital image of an assembled vessel.

To ensure a consistent environment for samples during the aging process, care was taken to affirm that assembled vessel seals did not leak. The manifold assembly shown in Figure 7 was used to check for possible gas leakage. With the assembled vessel attached to port (c) and a rotary pump connected to port (a), a vacuum was applied to the vessel with port (b) closed. Pressure in the vessel was monitored using a digital pressure gauge. When the pressure became lower than -14.5 psig, the ball valve on the vessel was closed and the vessel was detached from the manifold. To check if a leak occurred, the vessel was re-attached to the manifold after a period longer than 24 hours and the pressure in the vessel measured. If the pressure returned to atmospheric pressure (i.e., 0 psig), the vessel was considered to have a leak. In the case of a leak, the next step was to identify the leak location by immersing the vessel into water and supplying a continuous stream of nitrogen through the ball valve end of the vessel. At the location of the leak, the vessel connections were tightened. Then the vessel was reattached to the manifold and the process was repeated until all leaks were removed. After verifying no leaks within the vessels, the vessels were attached to the manifold with port (b) open to back-fill the vessels with approximately 14.6 psig of purified air. Initial polymer mass included in each vessel and corresponding pressure of zero air are shown in Table 5.

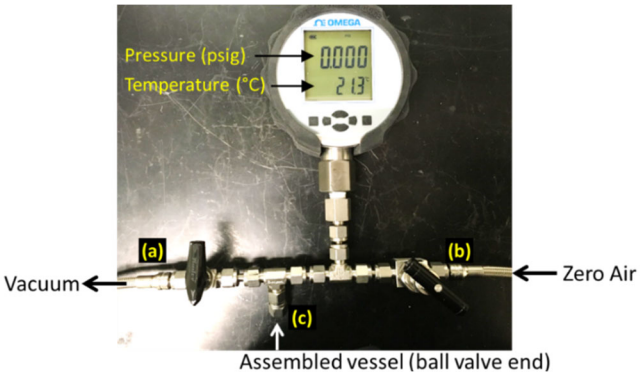

Figure 7. Manifold used to vacuum and back fill each of the assembled vessels.

Table 5. Average initial conditions of the insulation samples (n = 21) and gases in each vessel.

Number of Vessels	Solid				Gas		Target Aging Condition	
	Material	Mass* (g)	Density (g/ml)	Volume (mL)	Pressure (psig)	Volume (ml)	Temp (°C)	Dose Rate (Gy/hr)
21	XLPE	2.72±0.01	1.39±0.01	1.96	14.6±0.09	52.78±2.13	R.T.	100, 200, 300
21	EPR	3.05±0.02	1.23±0.01	2.47	14.6±0.04	52.65±1.25	R.T.	100, 200, 300

*Total mass of all samples sealed in the same vessel

3.3 Sample Aging

The sealed vessels containing the insulation samples in purified air were shipped to the Gamma Irradiation Facility (GIF) at Sandia National Laboratories. The layout of the inside of the sample irradiation room containing the assembled vessels is shown Figure 8. Vessels were placed in three rows, each at a different radial distance from the gamma source. Irradiation-only aging was carried out at ambient conditions (around 26°C). Unirradiated samples were also contained in vessels and sent to GIF for the duration of the experiment to ensure consistency between the test and control samples. The chosen target dose rates and irradiation times were up to 300 Gy/hr and 42 days, respectively, to achieve a maximum target dose of 3,000 kGy (30 Mrad) at the most severe exposure condition. Actual dose rates were measured using a calibrated cylindrical ionization chamber with an electrometer. Total doses are shown in Table 6.

Figure 8. Layout of the gamma irradiation chamber at Sandia National Laboratories.

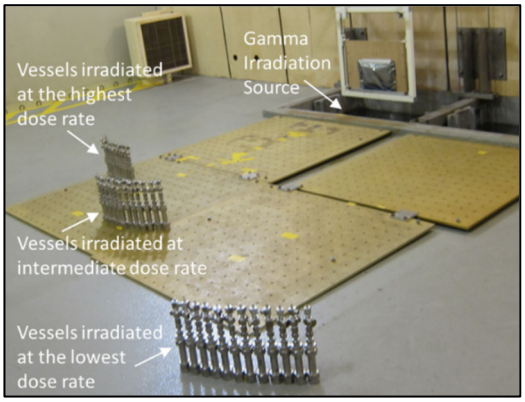

Table 6. Actual dose rates, aging times, and resulting total doses for aging conditions selected for XLPE and EPR.

	Dose Rate (Gy/hr)		
	102.96	209.52	316.08
Time (Days)	Total Dose (Mrad)		
6.80	1.68	3.42	5.16
13.60	3.36	6.84	10.31
20.40	5.04	10.26	15.47
27.20	6.72	13.67	20.63
33.99	8.40	17.09	25.79
40.79	10.08	20.51	30.94

4. CHARACTERIZATION

The primary focus of this study was to assess the effectiveness of oxygen consumption as a sensitive measure of aging (SMA) for cable insulation materials in comparison with other commonly employed measures of insulation aging. For this purpose, the five characterization methods introduced in this section were applied to evaluate aging in cross-linked polyethylene (XLPE) and ethylene-propylene rubber (EPR). For each method, the measured response, operating principle, and test procedure are described.

4.1 Measurement of Oxygen Consumption by Pressure-Volume-Temperature and Gas Chromatography

Oxygen consumption characteristics during degradation of polymers can provide meaningful insights into the aging process. In this work, oxygen consumption was closely examined as a method to characterize gamma radiation-induced aging in XLPE and EPR. The Pressure-Volume-Temperature (PVT) method in conjunction with gas chromatography (GC) was used to determine oxygen consumption values. PVT measurements were carried out twice: first, total pressure and temperature were recorded directly before a sample of gas was injected into the GC; second, the gas volume in a vessel was determined by pumping a known amount of gas into the vessel and measuring the resulting pressure. Total amount of gas was calculated using the ideal gas law,

$$PV = nRT \tag{3}$$

where, P, V, and T are the pressure, volume, and temperature of the gas; n is the number of moles and R is the universal gas constant (8.3145 $Jmol^{-1}K^{-1}$).

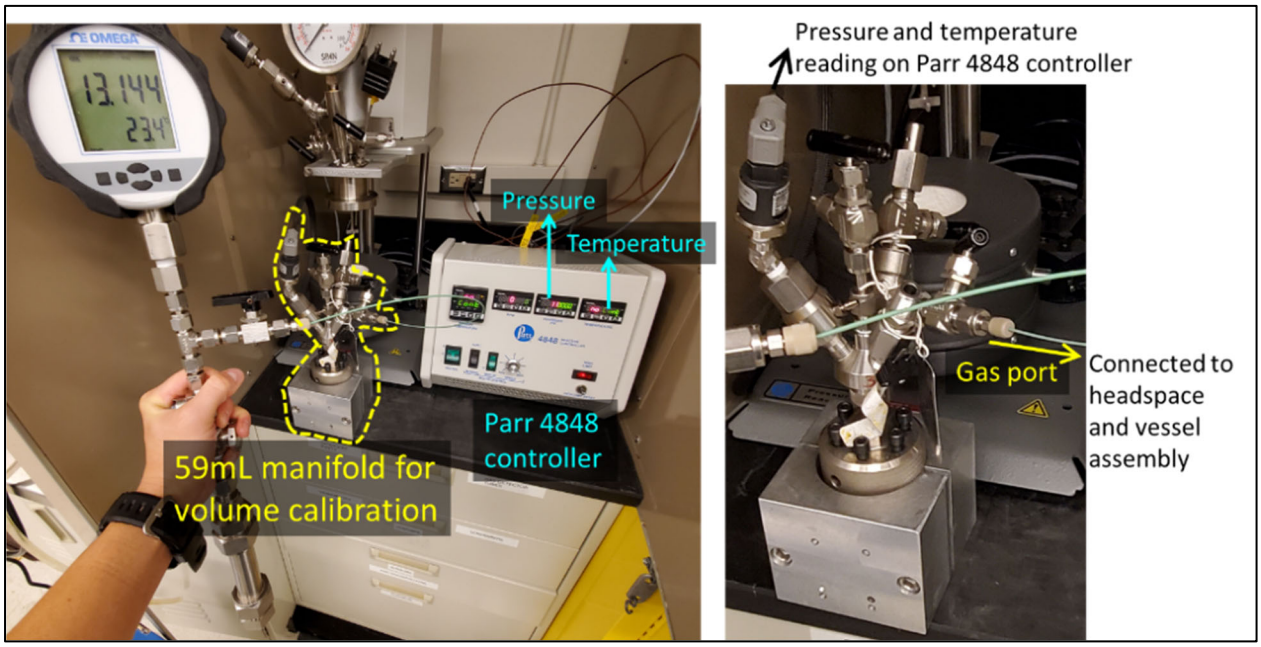

Figure 9. Calibrated 59mL manifold for volume measurement of gas inside vessel.

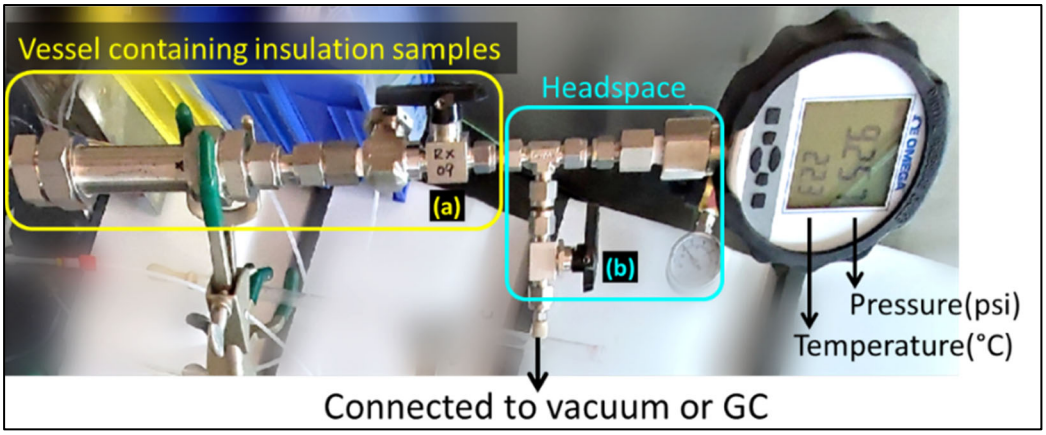

Figure 10. Manifold for pressure and temperature measurement of gas inside vessel.

To accurately measure the volume of gas in the vessel containing the insulation samples, the following procedure was used. The vessel was connected to a 59 mL standard calibration manifold (V_{cali} = 59 mL), which in turn was connected to a Parr 4848 reaction controller as shown in Figure 9. The sum of the vessel volume (V_{vessel}) and the headspace volume ($V_{headspace}$) was the total unknown volume (V_{unknown}) to be determined (see Figure 10). First, the pressure (P_{before}) and temperature of the evacuated assembly were measured using the Par 4848 controller. Next, 35 psig of purified air was pumped into the manifold and then introduced into the evacuated assembly (having volume = $V_{unknown}$). Following this, pressure (P_{after}) and temperature readings were obtained for the assembly after introduction of purified air (Table 4). As the temperature readings were constant during volume measurement, the volume for each vessel (V_{vessel}) was calculated using Equations (4) and (5),

$$V_{unknown} = \frac{P_{before}+P_{1atm}}{P_{after}+P_{1atm}} \times V_{cali} \quad (4)$$

$$V_{vessel} = V_{unknown} - V_{headspace} \quad (5)$$

where P_{before} and P_{after} are gauge pressures directly read on the Parr controller and P_{1atm} is the atmospheric pressure (14.7 psig). $V_{headspace}$ was measured following the same procedure, but with valve (a) in Figure 10 closed so that V_{vessel} is zero in Equation (5).

Once the number of moles of gas in each vessel was calculated, the molar fraction of each component in the gas mixture was measured using gas chromatography (GC). In this study, a 4-module INFICON micro-GC fusion gas analyzer was used. Gas from the vessel was drawn into the instrument, split, and injected onto the column with either argon (pre-purified, 99.9999%) or helium (ultra-high purity, 99.9999%) as the carrier gas. Two porous layer open tubular (PLOT) columns (Restek®) were used to separate gas components based on their polarity and to identify them based on their retention time. The column media were molecular sieve ("Rt-Molsieve 5Å") for Module A and divinylbenzene ethylene glycol/dimethylacrylate ("Rt-U-BOND") for Module B. A microelectromechanical system-based micro thermal conductivity detector (μTCD) was used to identify the gases. A 3-level calibration was applied to the columns using a mixture of standard gases (H_2, O_2, N_2, CO, CH_4, and CO_2) obtained from OXARC® as primary standards.

4.2 Measurement of Mass and Density

The mass of each insulation sample was measured using an analytical balance (Mettler Toledo XPR205, 0.01 mg readability), as shown in Figure 11. Sample density was measured using the same analytical balance shown in Figure 11, but equipped with a density kit following ASTM D792 (ASTM D792-20, 2020). 5 mm-long samples were bisected along their length to eliminate bubble formation on the interior diameter of the hydrophobic insulation samples. Samples were pre-conditioned following ASTM D618 at 23°C ± 2°C and 50% ± 10% relative humidity for more than 40 hours prior to density measurement (ASTM D618-21, 2021). Mass of the samples in air (m_{air}) was first measured. Next, the samples were wetted with isopropanol alcohol (IPA) to lower surface tension at the polymer-water interface where bubbles may form and cause the measured density to be lower than the true value. The samples were then placed on a convex sample holder and immersed in deionized water. Care was taken to ensure no bubbles were trapped in the hollow center of the samples. The apparent mass of samples in water (m_{water}) was then recorded. It was assumed that the trace amount of IPA on the sample surfaces would not cause the density of liquid to deviate from the density of water. According to the Archimedes' principle, the difference between air mass and underwater mass is due to buoyancy of water that would otherwise occupy the submerged volume. Therefore, the density of the samples was calculated using Equation (6). Measurements were performed in triplicate and the temperature of the water was accounted for using a thermometer.

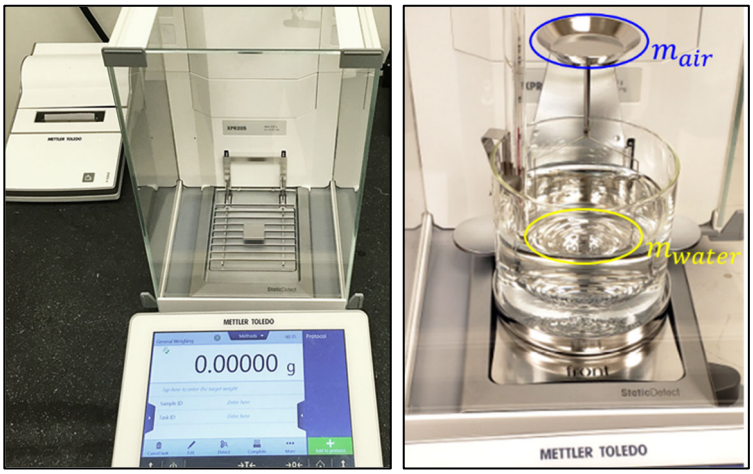

Figure 11. Analytical balance and density measurement kit.

$$\rho_{sample} = \frac{m_{air}}{V_{sample}} = \frac{m_{air}}{m_{air} - m_{liquid}} \times \rho_{liquid} \quad (6)$$

4.3 Measurement of Carbonyl Index by Fourier Transform Infrared Spectroscopy

FTIR may be used to identify chemical changes in materials through tracking of absorption intensities at characteristic absorbance energies. This technique enables the determination of the carbonyl index (CI), which is a measure of the conversion of C-C or C-H bonds to carbonyl (C═O) bonds due to oxidation. In this work, CI was measured for XLPE and EPR to track oxidation occurring as a result of the aging process and for comparison to O_2 consumption.

Characterization of XLPE and EPR insulation samples was carried out using a Bruker Alpha II OPUS Touch FTIR spectrometer equipped with an attenuated total reflection (ATR) attachment as shown in Figure 12. A 10 mm-long sample was cut and extracted from the end of each insulation sample prior to FTIR measurement. These extracted samples were pre-conditioned in a controlled environment of 23°C ± 2°C

and 50% ± 10% relative humidity for at least 40 hours. Humidity was controlled by placing the samples in a covered desiccator charged with a saturated solution of potassium carbonate and deionized water. Following conditioning, individual samples were placed centered on the diamond ATR crystal. For every sample, 64 scans were collected at a resolution at 4 cm^{-1} to minimize signal variation due to random noise. Three replicate measurements were taken per sample.

After testing, analysis of the collected FTIR spectra was performed using the hyperSpec package in R (Beleites and Sergo, 2013). Carbonyl index (CI) was determined as the ratio between the band absorbance intensity of the carbonyl peak (at 1715 cm^{-1}) ($A_{C=O}$) and that of the methylene symmetric stretch peak (between 2846 and 2850 cm^{-1}) (A_{C-H}) as shown below in Equation (7).

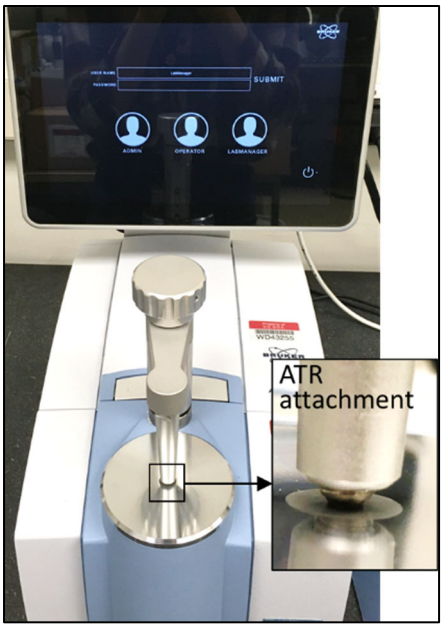

Figure 12. Experimental set up for FTIR analysis using an ATR attachment.

$$CI = \frac{A_{C=O}}{A_{C-H}} \tag{7}$$

4.4 Measurement of Yellowness Index by Image Analysis

Color change of polymers may occur as a consequence of chemical changes on the polymer surface and yellowness index is a standard industrial measurement to quantify the visual ratings of color change. Following ASTM D1729 and ASTM D2244, the yellowness index (YI) of the XLPE and EPR samples was measured using a GTI MiniMatcher MM-2e viewing system with a CIE Standard Illuminant D65 light source and Nikon D7500 digital camera (ASTM D2244-16, 2016; ASTM D1729-16, 2016). The camera was mounted on a stand and oriented perpendicular to the display panel as shown in Figure 13. To optimize the quality of the collected images, the camera parameters used were as follows: 1/250 s exposure time to enhance color saturation and f5 aperture to enhance depth of field. Furthermore, background lighting in the room was extinguished during image collection to minimize interference from other light sources. A wireless remote control (Nikon ML-L3) was used to ensure the camera orientation was not disrupted during image collection. Three replicate photos were acquired for each sample, where the sample was rotated and flipped between replicates to minimize deviation caused by differences in light condition and camera angle at different pixel positions within a frame.

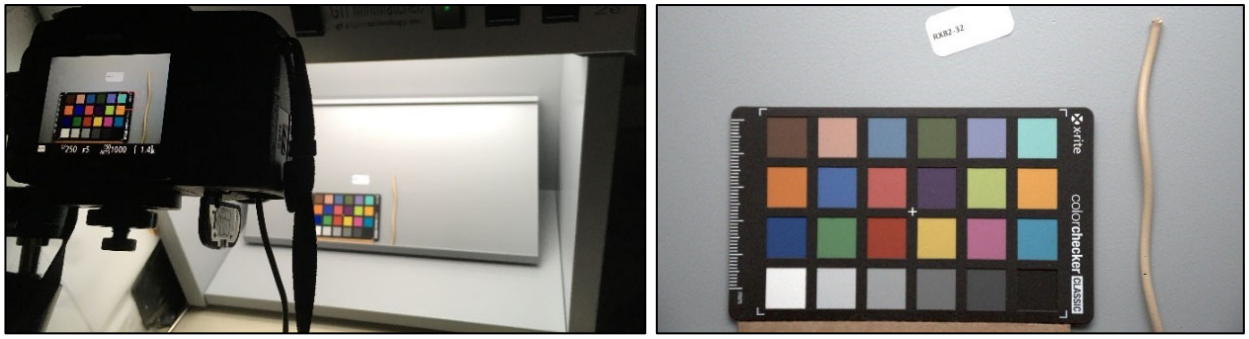

Figure 13. (Left) Experimental set up for image analysis and (right) a digital image of XLPE sample next to the color checker.

A digital camera lens will modify the color in recorded digital images as a result of inherent components and internal processing mechanisms. Therefore, it is necessary to map these modified colors into a system with an absolute measure of color prior to quantifying color changes. NIH ImageJ software was used in conjunction with the micaToolbox plugin to convert the collected images to the CIEXYZ color space. First, the 6 grey standards located on the bottom row of the color checker (shown in Figure 13) were converted to reflectance values using manufacturer-supplied standard Red Green Blue (sRGB) triplets for each grey standard. Next, an iterative least log slope approach was used to convert the triplets to reflectance values. Then, the grey reflectance values were used to create a linear normalized reflectance stack, or calibrated multispectral image, for each collected image. Following this, regions of interest (ROIs) were manually specified for each calibrated image, over which the averaged X, Y, Z values were determined. Care was taken to select regions with no reflections or shadows. Two ROIs were selected for each image to obtain a total of 6 data points for each aging condition. A cone-catch model was then generated based upon the charted reflectance spectra of the 24 reference colors on the color checker. The cone-catch model was used to map the linear normalized reflectance stack to the CIEXYZ color space and the X, Y, Z values of saved ROIs were measured. Lastly, the measured X, Y, Z values were mapped to D65 reference white point CIELAB color space through the built-in MATLAB function *xyz2lab*. Average YI results were determined based on Equation (8) for each irradiation condition,

$$YI = \frac{100(C_X X - C_Z Z)}{Y} \tag{8}$$

where C_X = 1.2985 and C_Z = 1.1335 for D65 illuminant and CIE 1931 observer (2°), and X, Y, Z are the CIE tristimulus values obtained by photo analysis.

5. RESULTS

In this section, all characterization data with a focus on time (and dose) dependency of material properties are presented. Oxygen consumption is compared to other common measures of polymer aging. It was assumed that samples harvested from the same batch were equivalent.

5.1 Oxygen Consumption

Net change in the amount of oxygen ($-\Delta n_{O_2}$) in each vessel was calculated based on PVT data and GC results using Equation (9). Oxygen consumption (OC) was then calculated by normalizing the net change in the amount of oxygen by the mass of the polymer in the vessels as shown in Equation (10),

$$-\Delta n_{O_2} = \left(\frac{p^i}{T^i} x^i_{O_2} - \frac{p^f}{T^f} x^f_{O_2}\right)\frac{V}{R} - S\left(p^f x^f_{O_2} - p^i x^i_{O_2}\right) \tag{9}$$

$$OC = \frac{-\Delta n_{O_2}}{m} \tag{10}$$

where superscripts i and f stand for initial (before aging) and final (after aging), respectively, p the total pressure of the purified air, T is the temperature, V is the volume of gas inside the vessel, x_{O_2} is the gas fraction of oxygen, S is the solubility of oxygen within the polymer, and m is the mass of all insulation samples sealed within the same vessel. The second term on the right-hand side of Equation (9) accounts for dissolved oxygen in the polymer samples. Here, the contribution of solubility is negative because dissolved oxygen was released during aging (Seguchi and Yamamoto, 1986). Although oxygen change due to solubility was negligible (-0.3% for XLPE and -0.7% for EPR), results in Section 5.1 include solubility corrections.

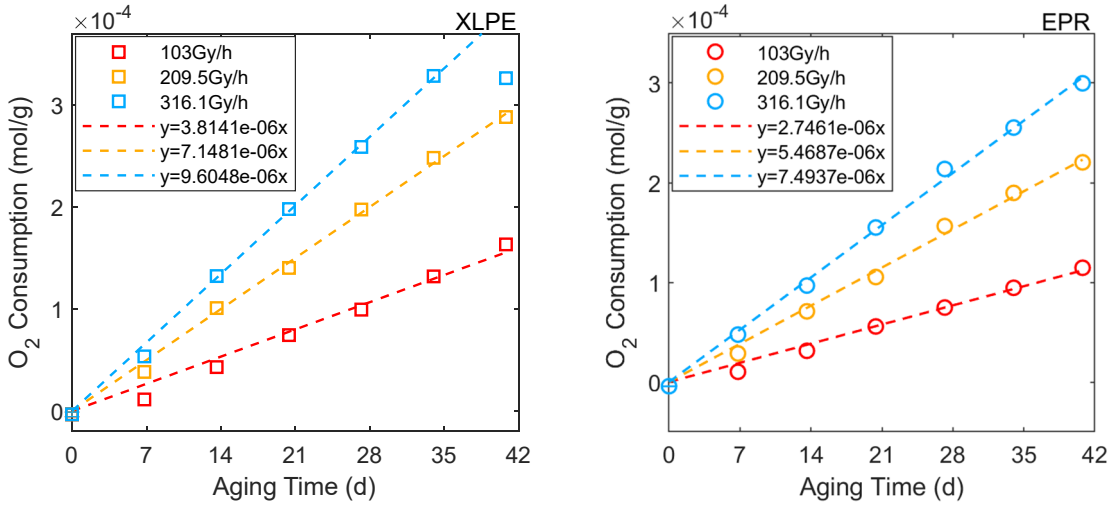

Figure 14. Oxygen consumption plotted as a function of aging time for XLPE and EPR samples irradiated at three dose rates indicated in figure legends.

Figure 14 shows Equation (10) as a function of irradiation time for XLPE and EPR subjected to the 3 gamma irradiation dose rates. Oxygen consumption was observed to increase linearly with aging time for all points of all studied samples, except for one data point at the most severe irradiation condition (300 Gy/h and 42 days, or 30 Mrad) for XLPE. In that instance it is hypothesized that all oxygen inside the vessel had been consumed at that extreme irradiation condition so that the measured oxygen consumption value was

artificially deflated. As a result, the 42-day data point at an irradiation rate of 316.1 Gy/h for the XLPE sample was not included in further analysis.

$$\phi = \frac{d(OC)}{dt} = \frac{-\Delta n_{O_2}}{m\Delta t} \tag{11}$$

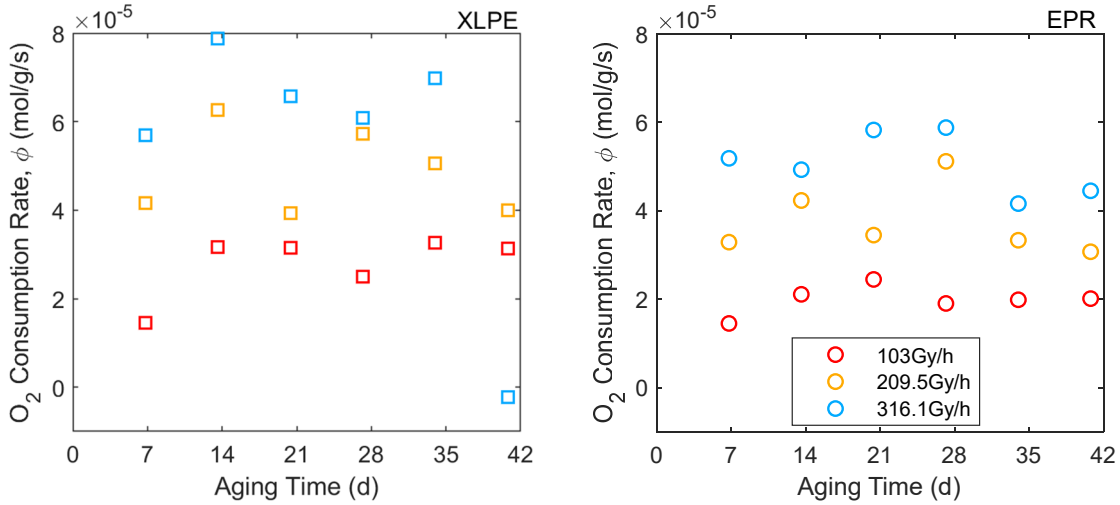

Figure 15. Oxygen consumption rates plotted as a function of aging time for XLPE and EPR samples irradiated at three dose rates indicated in figure legends. No error bars since there is only one vessel of samples per condition.

Piecewise OC rates (ϕ) were calculated by dividing the increment in OC by the aging time interval Δt, see Equation (11). Note that the OC rate (ϕ) is defined differently from r_{O_2} in Equation (2) as ϕ is normalized by the polymer mass. As shown in Figure 15, ϕ was generally constant despite some fluctuation. The average OC rates were calculated by linear regression of OC vs. time over the entire aging period (Δt = 42 days) and results are reported in Table 7. Average OC rates with respect to total dose are also reported in Table 7 using the linear regression method as shown in Figure 16. Dose rate effects were not found to be significant in this work as seen in Figure 16 where the OC at different dose rates can be superimposed when plotted against total dose.

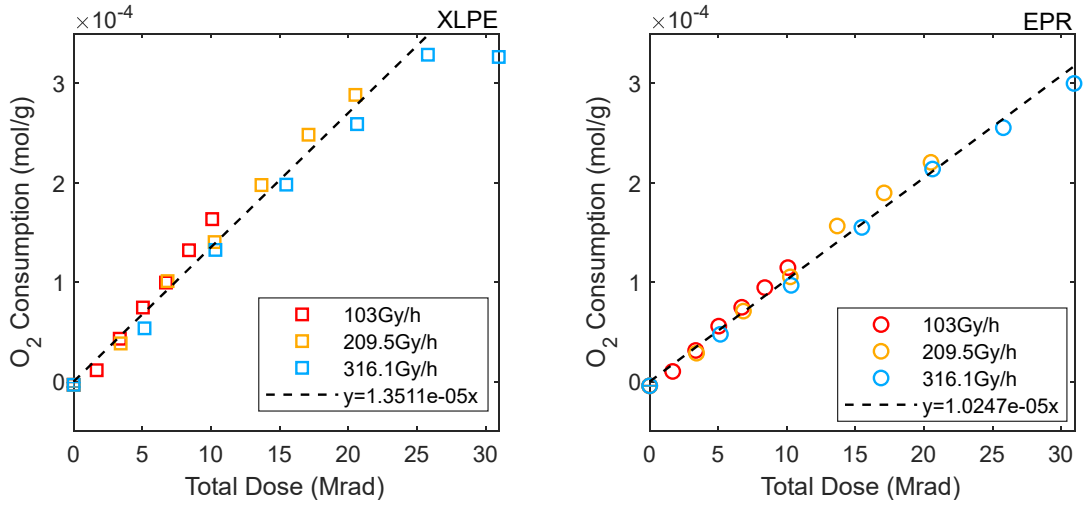

Figure 16. Oxygen consumption plotted as a function of total dose (in Mrad) for XLPE and EPR samples irradiated at three dose rates indicated in figure legends.

Validation of the techniques and results presented in this work was performed through comparison to published studies. In general, reported OC rates for XLPE and EPR-based insulations range from 5 x 10^{-10} to 1.4 x 10^{-9} mol/g/Gy at dose rates ranging from 5 to 2000 Gy/h and aging temperatures up to 70°C. Oxygen consumption rate values determined in this work (see Table 7) are in good agreement with published results, although possibly trending towards the higher end (1 x 10^{-9} mol/g/Gy) of historical data. A detailed comparison can be found in Section 0.

Table 7. Calculated average oxygen consumption rate ϕ for each irradiation dose rate and overall average ϕ for each material investigated in this work.

Material	ϕ (mol/g/s)			ϕ (mol/g/Gy)
	316.1 Gy/h	209.5 Gy/h	103.0 Gy/h	
XLPE	1.11E-10	8.27E-11	4.41E-11	1.35E-9
EPR	8.67E-11	6.33E-11	3.18E-11	1.02E-9

5.2 Mass and Density

Mass change is a common technique used to assess and predict the degradation of polymeric materials (Sarrabi *et al.*, 2009). Typically, an increase in mass is correlated with polymer oxidation. Within this work, it was observed that mass increased linearly with exposure time as shown in Figure 17 and Figure 18. Furthermore, it was observed that the results obtained at the three investigated dose rates overlap when plotted against total dose, similar to trends observed in oxygen consumption data. Good linearity was also observed for all samples, except for the highest aging time for the XLPE samples. This deviation was attributed to the consumption of all available oxygen as mentioned in Section 5.1.

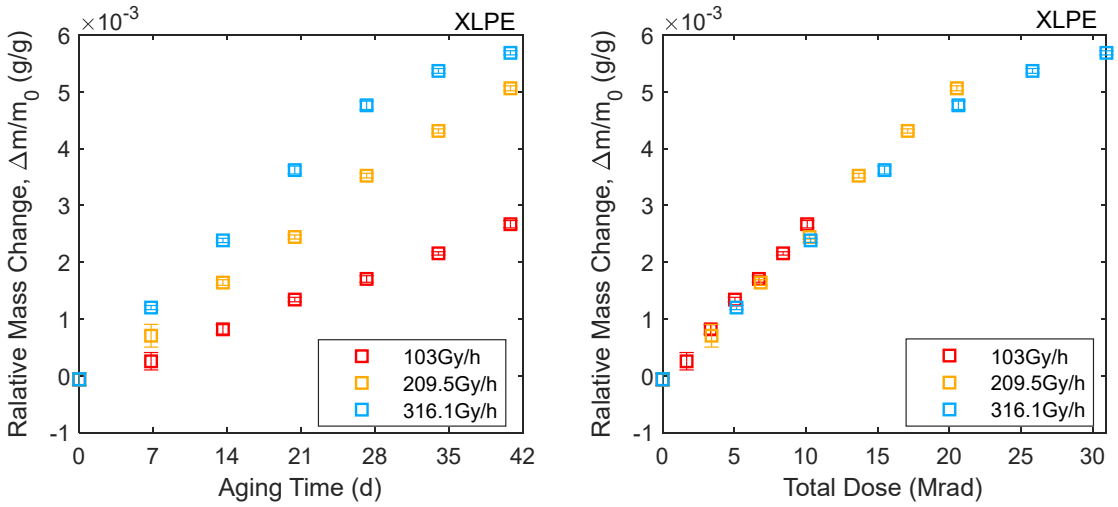

Figure 17. Normalized mass change plotted as a function of (left) aging time and (right) total dose for XLPE samples irradiated at three dose rates indicated in figure legends.

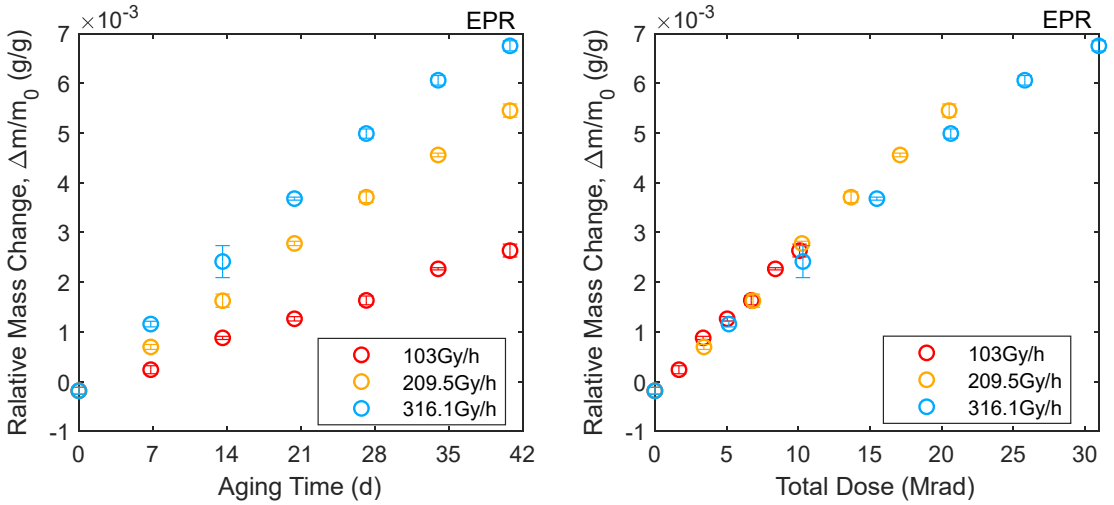

Figure 18. Normalized mass change plotted as a function of (left) aging time and (right) total dose for EPR samples irradiated at three dose rates indicated in figure legends.

Another common, and complimentary measurement to mass, is density change (Gillen, Celina and Clough, 1999). Importantly, density may not be as sensitive a measure of aging as mass in a given situation as the homogeneity of oxidation reactions across a sample may significantly affect observed density differences. Within this work, it was observed that average density values of the insulation samples remained constant with exposure as shown in Figure 19 and Figure 20. Diffusion limited oxidation may have contributed to keeping the average density value consistent throughout the irradiation process as sample density predominantly depends on the interior volume, which is hypothesized not to change in a diffusion limited oxidation scenario. Alternatively, it is hypothesized that the consistent observed values of density may have resulted from the additive combination of increase in density due to polymer chain cross-linking and decrease in density from polymer chain scission.

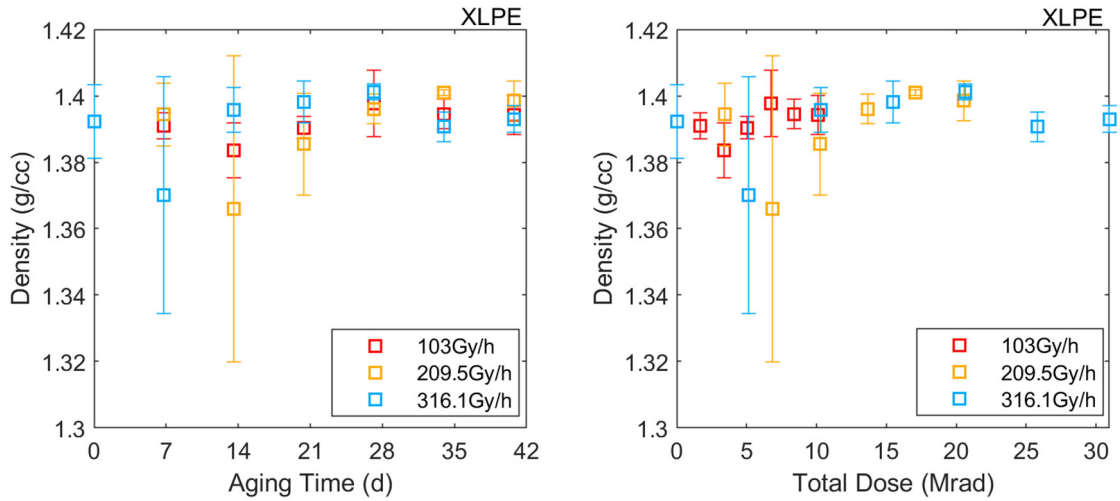

Figure 19. Observed changes in density as a function of (left) aging time and (right) total dose for XLPE samples irradiated at three dose rates indicated in figure legends.

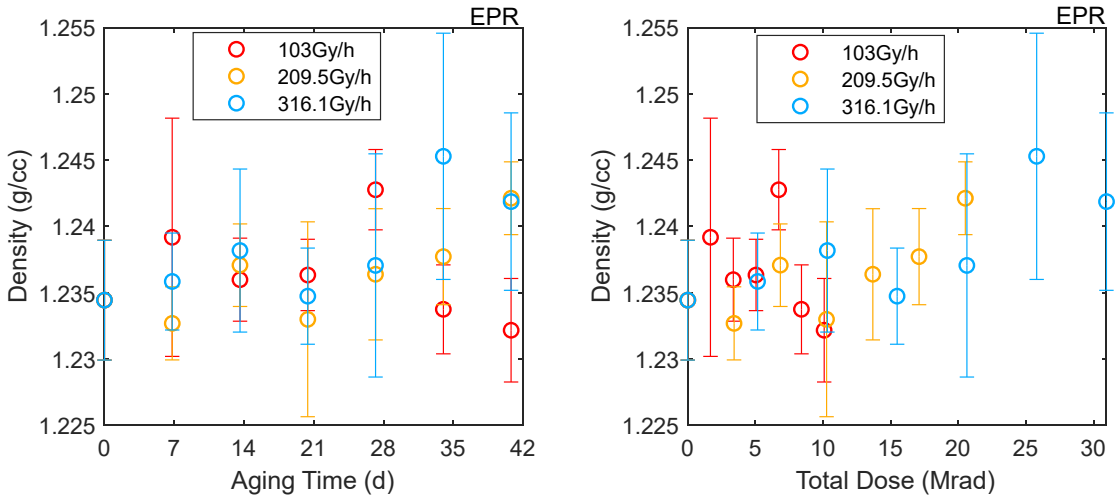

Figure 20. Observed changes in density as a function of (left) aging time and (right) total dose for EPR samples irradiated at three dose rates indicated in figure legends.

5.3 Carbonyl Index and Yellowness Index

Carbonyl index is another commonly used method to track aging of polymers (Feller *et al.*, 2007). Carbonyl index (CI) values were calculated from FTIR measurements on the surface of the irradiated samples as discussed in Section 4.3. A complimentary analytical method is yellowness index (YI) which tracks chromophore changes occurring on the surface of polymer samples that result in apparent and measurable discoloration. These chemical changes are commonly attributed to the formation of conjugated bonds within the polymer macrostructure (Wypych, 2020).

Time-dependent CI curves obtained at the three dose rates for the XLPE samples are reported in Figure 21. It was observed that the trends were superimposable when standard deviations were considered. Furthermore, it was observed that CI exhibited a linear increase as a function of total dose, although the slope of the linear lines of best fit varied slightly between measured dose rates. Assuming that the concentration of alkyl groups is constant, which is a reasonable assumption in polyolefin-based materials, the linear time (or total dose) dependence indicates that carbonyl groups continue to accumulate throughout the exposure times and total doses investigated in this work.

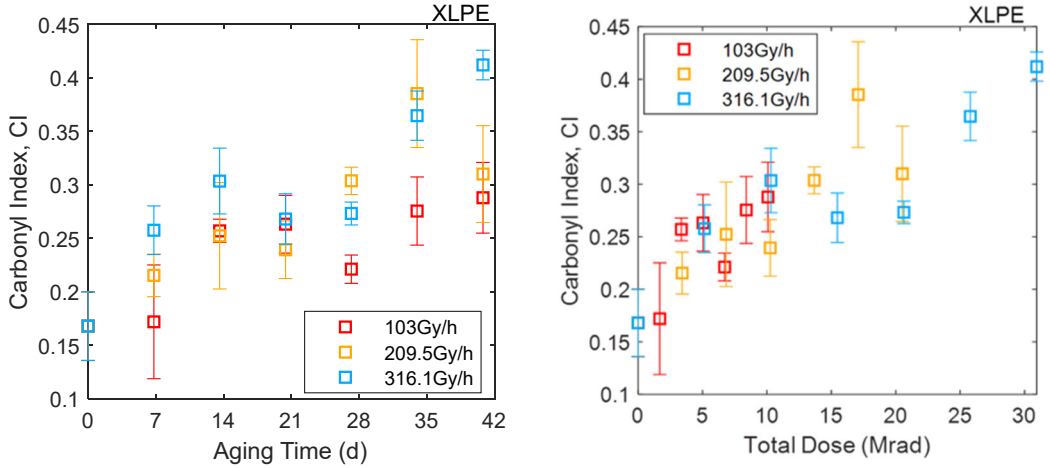

Figure 21. Calculated changes in CI as a function of (left) aging time and (right) total dose for XLPE samples irradiated at three dose rates indicated in figure legends.

Yellowness index was only measured for the white-colored XLPE samples in this work as YI is less reliable for black-colored samples, such as the EPR selected herein. Calculated YI of XLPE was plotted as a function of irradiation time and total dose and is shown in Figure 22. A logarithmic time (or total dose) dependence was observed, suggesting a saturation of oxidation reactions at the sample surfaces towards the later irradiation stages investigated in this work. The difference in trends when comparing YI to CI was not unexpected, as YI measures changes on visible light absorption (100s of nanometers) and CI relies on far infrared light absorption (several micrometers). CI is therefore expected to evolve for longer durations than YI as YI is entirely a surface dependent measurement.

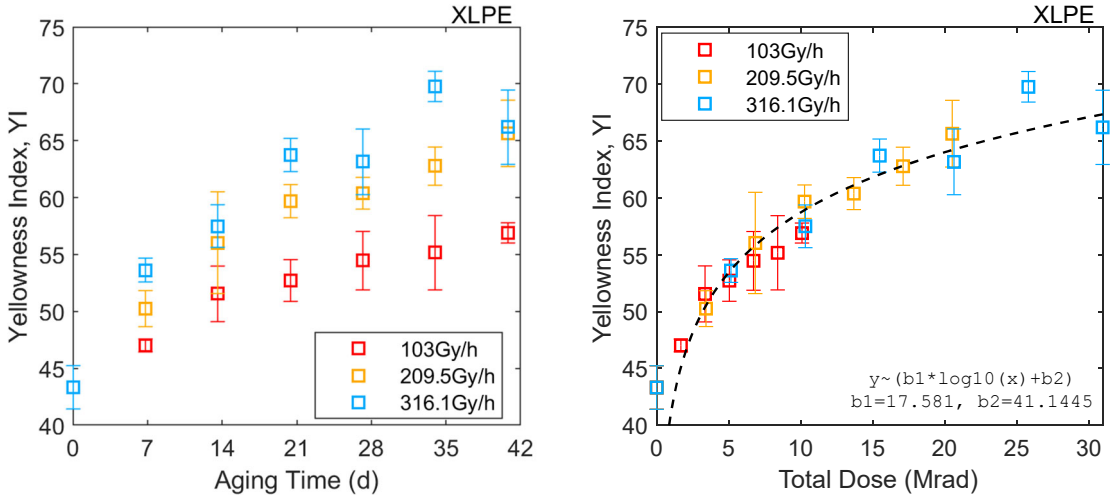

Figure 22. Calculated changes in YI as a function of (left) aging time and (right) total dose for XLPE samples irradiated at three dose rates indicated in figure legends.

Time-dependent CI curves obtained at three dose rates for EPR samples are reported in Figure 23. It was observed that CI of EPR increased approximately linearly throughout the irradiation process. Deviations from linearity were found to be within the range of error for the measurements.

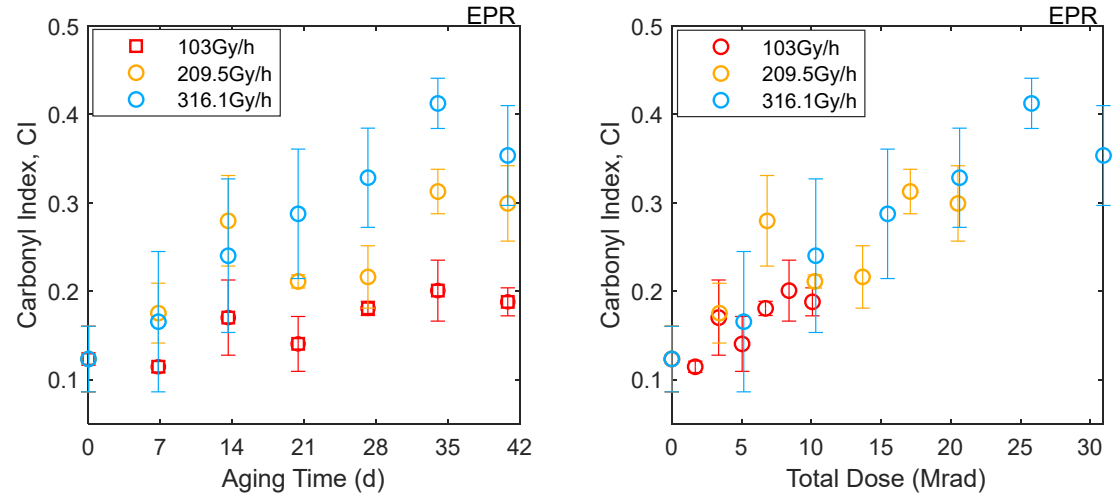

Figure 23. Calculated changes in CI as a function of (left) aging time and (right) total dose for EPR samples irradiated at three dose rates indicated in figure legends.

6. DISCUSSION

Sensitive measures of aging (SMA), analytical techniques that can detect material degradation under relatively mild conditions, may be useful in predicting material performance at conditions where traditional material lifetime prediction metrics do not provide useful information. In this work, oxygen consumption (OC), a promising candidate SMA, was compared to traditional material performance metrics and evaluated for two common types of cable insulation materials, crosslinked polyethylene (XLPE) and ethylene-propylene rubber (EPR). To facilitate comparison between candidate techniques, OC, mass change (Δm), density (ρ), carbonyl index (CI) and yellowness index (YI) analytical results reported in Section 5 were mapped to the same axes by min-max normalization (see Figure 24 for XLPE and Figure 25 for EPR).

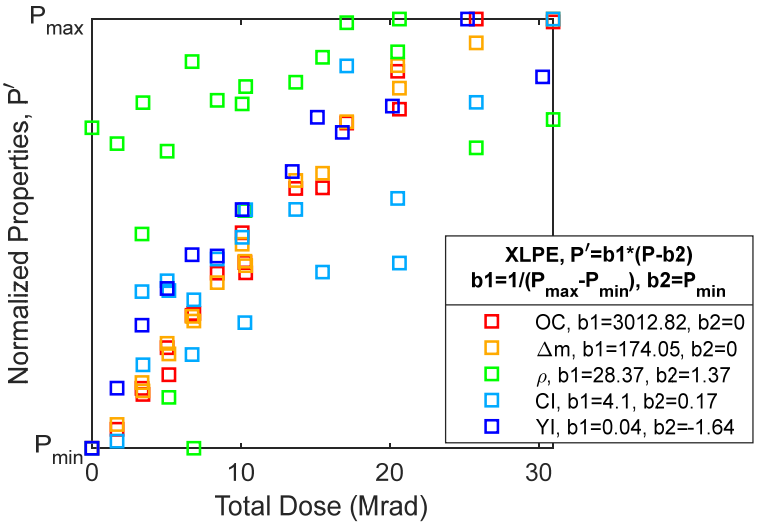

Figure 24. Rescaled material responses for XLPE versus total dose by min-max normalization. The rescaling factors are given in the figure caption.

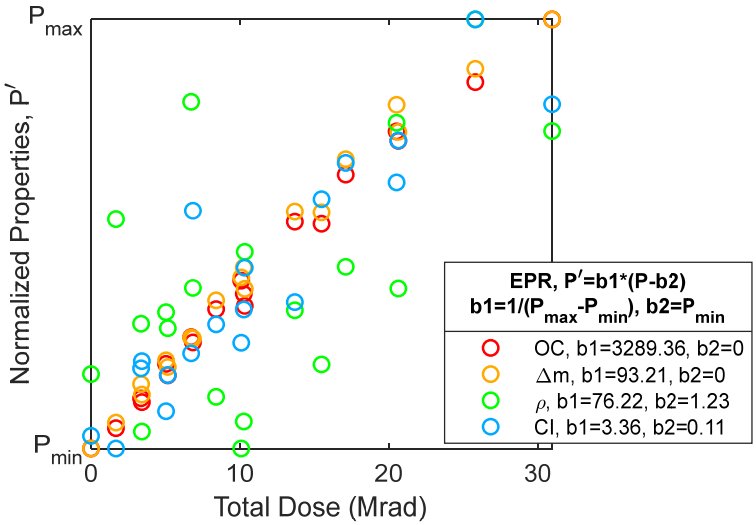

Figure 25. Rescaled material responses for EPR versus total dose by min-max normalization. The rescaling factors are given in the figure caption.

Mass change was found to linearly track with time and dose with small deviations as shown in Section 5.2, making it a potentially a good SMA candidate. In fact, the linear dose dependence of mass gain is an expected result from the mass balance between solid and gas phases inside the airtight vessel. To check if the source of mass gain in the solid phase was consumption of oxygen gas, mass change in the gas phase was calculated following Equation (12), where the changes in molar amounts (Δn) of gaseous byproducts are given in Section 9.1.

$$\Delta m(gas) = \Delta n_{O_2} \times \frac{32g}{mol} + \Delta n_{CO_2} \times \frac{44g}{mol} + \Delta n_{CO} \times \frac{28g}{mol} + \Delta n_{H_2} \times \frac{2g}{mol} + \Delta n_{CH_4} \times \frac{16g}{mol} \quad (12)$$

As shown in Figure 26, mass changes in gas and solid phases overlap up to 10 Mrad for XLPE and up to 20 Mrad for EPR, above which the mass gain in solid phases falls behind the mass loss of the gases. Deviation from a balanced mass change renders mass change an SMA only in the early degradation stage, i.e., below 10 and 20 Mrad for the investigated XLPE and EPR, respectively.

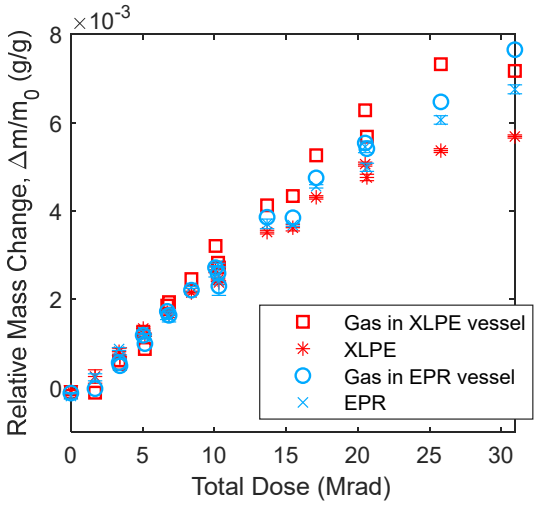

Figure 26. Normalized mass changes in XLPE and EPR samples and surrounding gas phases sealed in the aging vessel.

Density values of polymers are known to change after irradiation and/or oxidation. (Gillen, Celina and Clough, 1999). Interestingly, no significant changes in density were observed in either XLPE or EPR samples in this work. This suggests that density as a measure of polymer aging is not sensitive to sample degradation during the early stages of irradiation investigated herein. In contrast, YI exhibited sigmoidal evolution with total exposure dosage for XLPE samples, somewhat similar to the linear trends calculated for oxygen consumption. It was therefore concluded that these techniques are similarly sensitive to the early stages of degradation probed in this work. However, changes in YI were observed to stagnate as total exposure dosage approached 30 Mrad. This was attributed to the exhaustion of available moieties on the surface of cable insulation samples that can oxidize into the conjugated bonds responsible for polymer yellowing during irradiation. Because YI is so surface sensitive, the technique may not be a suitable SMA. In contrast, oxygen consumption continued to evolve linearly through a 30 Mrad total exposure dosage.

Carbonyl index is a further technique that is readily available for the analysis of polymer oxidation. A strength of CI relative to YI is its increased penetration depth. It was observed that CI evolved linearly with total dose rate similarly to OC, again demonstrating that OC is a suitable technique for quantifying polymer aging. However, CI can be limited in certain polymer formulations by the overlap between absorption peaks due to polymer oxidation and those due to antioxidants added to the polymer in production. OC, on the other hand, is not so limited. Importantly, in this study OC was observed to evolve linearly in all investigated irradiation scenarios, which was identified as a key parameter for the validity of OC as an SMA and permits its usage for E_a and lifetime prediction calculations.

6.1 Use of Oxygen Consumption Rates as an Alternative to Time-Temperature Superposition for Cable Lifetime Prediction

In this section, the question of whether shift factor a can be directly evaluated from oxygen consumption rate ϕ measured at different temperatures will be examined, i.e., if it is possible to have $a = \phi(T_2)/\phi(T_1)$ by comparing $\log_{10}(\phi)$ vs. $\log_{10}(a)$. In addition, calculation of activation energy (E_a) by OC will be directly compared to calculation of E_a by the more traditional elongation at break (EAB) approach using literature data. This approach could save significant time and effort when predicting material lifetimes by extrapolating from higher-than-service temperatures. As described in Section 1, estimation of service life of polymeric cable insulations is commonly based on Arrhenius temperature dependence where the E_a is parameterized from time-temperature superposition (TTS) of isotherms. The following example demonstrates the procedure to determine E_a without TTS using OC data. Since corresponding EAB values for the data presented in Section 5 were not available, the demonstration below uses previously published data from Sandia National Laboratories (Assink, Gillen and Bernstein, 2005). The same analysis may be performed using any dataset including isotherms of a material property (such as CI, YI, density, or EAB) and the OC rate at investigated temperatures. P/P_0 represents a generic normalized material property.

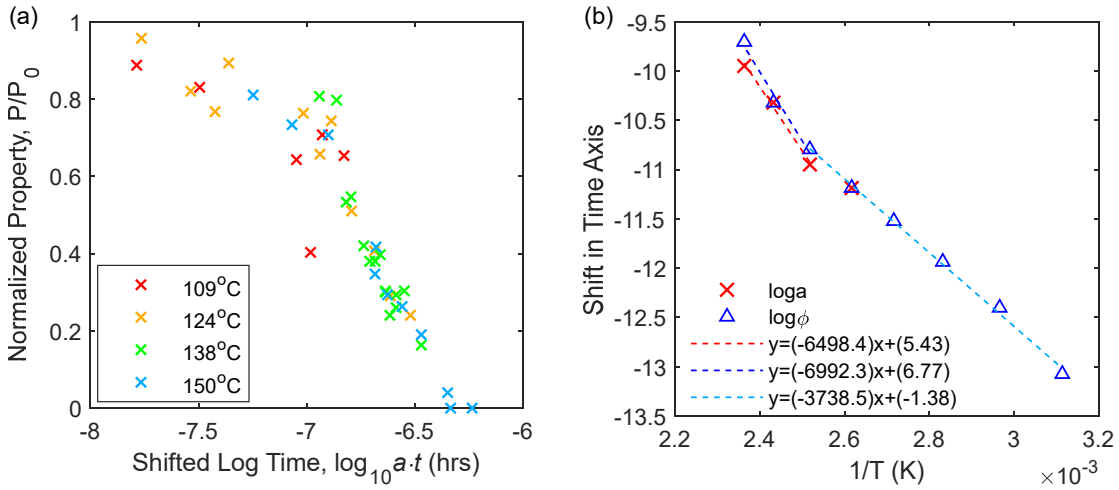

Figure 27. (a) Normalized master curve constructed by time-temperature superposition of four isotherms obtained from a literature dataset for an XLPO-based insulation sample. (b) Shift factors to create the master curve shown in (a) and oxygen consumption rates as a function of reciprocal absolute temperature.

The "master curve" obtained through conventional TTS by best-fit overlapping of the decreasing portion of P/P_0 isotherms is shown in Figure 27 (a). (It is noted that the isotherm at 109 °C does not monotonically decrease with time, rendering two possible shift factors at 109 °C. One of the two possible shift factors was selected based on the trend at the longest time.) The $\log_{10}(a)$ shift factors are plotted against the reciprocal absolute temperatures 1/T in Figure 27 (b) and exhibit good linearity excluding the outlier $\log_{10}(a)$ at 109°C. In the temperature range of 124 to 150 °C, the Arrhenius relationship holds true for the selected P/P_0 dataset. Also plotted in Figure 27 (b) are $\log_{10}(\phi)$ reported for the same material. Note that $\log_{10}(a)$ and $\log_{10}(\phi)$ at 138°C were normalized to compare the slopes of these two curves. This setting is equivalent to a change of reference temperature in TTS.

Despite the shift uncertainties caused by data scatter and isotherm shape changes, $\log_{10}(a)$ obtained from conventional TTS method and $\log_{10}(\phi)$ directly obtained from OC experiments are consistent over the temperatures (109 to 150 °C). Further examination of the comparability of these quantities would require P/P_0 isotherms at lower temperatures and exponentially longer aging times. At 109 °C, the aging time was 1.8 years, just surpassing the induction period. It is impractical to explore the P/P_0 behavior below 109°C

through mechanical testing due to long induction periods, whereas ϕ is measurable within several weeks of aging even at 'low' aging temperatures. Furthermore, $\log_{10}(\phi)$ vs. 1/T demonstrated good linearity within two temperature ranges: 124 to 150 °C and 48 to 124 °C, which suggests that the Arrhenius temperature dependence is a valid assumption. However, a clear decrease in slope was observed below 124°C. Correspondingly, E_a decreased as listed in Table 8.

Table 8. Activation energies calculated from the slopes of linear regression in Figure 27 (b).

Method	Temperature Range (°C)	Slope	Ea (kJ/mol)
TTS $\log_{10}(a)$	124-150	6498.4	124.4
OC $\log_{10}(\phi)$	124-150	6992.3	133.9
OC $\log_{10}(\phi)$	48-124	3738.5	71.6

As given in Table 8, the E_a values at 124 to 150°C determined by conventional TTS and alternative OC methods differ by only 7%. Considering the variability of approximately 15% to 30% in TTS-determined E_a based on endpoint selection, the 7% difference between methods indicates that the OC method provides comparable results. Given the significant experimental time reduction provided by OC, this supports its usage for cable lifetime prediction studies as OC is also capable of validating the Arrhenius assumption at lower temperature ranges where a decrease in E_a is commonly observed for polymeric materials (Gillen, Celina and Bernstein, 2003; Celina, Gillen and Assink, 2005; Gillen, Bernstein and Celina, 2005). Since the lowest temperature in the OC dataset was closer to the service temperature of cables, the E_a determined from $\log_{10}(\phi)$ at lower temperatures was perhaps more representative of service performance when predicting service lifetime.

When using OC rates for an XLPO-based insulation aged at 38 Gy/h and various temperatures from 40°C to 110°C, the Arrhenius relation could be examined by plotting $\log_{10}(\phi)$ against the reciprocal absolute temperature 1/T as shown in Figure 28. A linear relationship was observed above 60°C (i.e., the temperature-dominant region), indicating Arrhenius-type temperature dependence was valid and E_a can be determined from the slope of linear regression. However, deviation from Arrhenius behavior was observed at 40°C which was attributed to the transition from temperature-dominant to irradiation-dominant degradation. Further work is required to further understand the potential and limits for use of OC for lifetime prediction in combined stress aging environments.

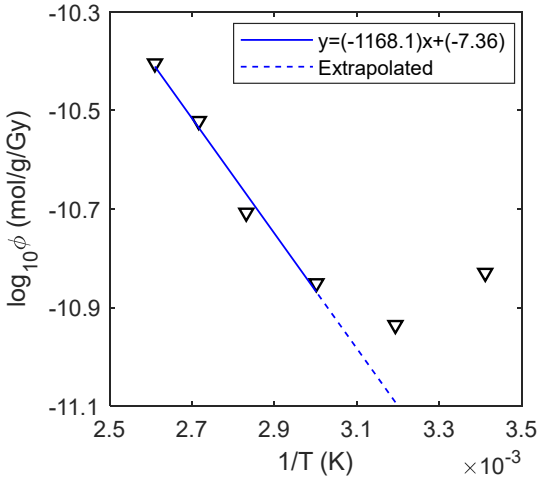

Figure 28. Oxygen consumption rates as a function of reciprocal absolute temperature for an XLPO-based insulation sample aged at combined thermal and irradiation conditions.

6.2 Material Property Changes During Aging on an Oxygen Consumption Coordinate

A primary use of oxygen consumption data is to shift the curves of the data vs. time on a log-log plot and obtain shift factors *a*, similar to the method used to calculate E_a from elongation-at-break (EAB) datasets (Gillen, Celina and Keenan, 2000; Calmet *et al.*, 2002; Gillen, Celina and Bernstein, 2003; Gillen *et al.*, 2006; Celina, Dayile and Quintana, 2013). For cable useful life prediction, it is necessary to relate OC values of insulation performance to endpoints (such as EAB = 50%) by measuring OC and metrics with defined endpoints under common conditions.

Example correlation between OC and other polymer aging analytical techniques is given in Figure 29, where a second x-axis was plotted using the overall OC rate calculated in Table 7. Use of OC as the x-axis is inherently consistent with the superposition concept described in Section 1. The form factor $a = t_1/t_2$ in Figure 1 and Equation (1) is evaluated as $a = \phi(I_2)/\phi(I_1)$. In this case, the form factor can also be evaluated by dose rates, $a = I_2/I_1$, since the dose rate independent assumption has been validated in Section 5. Thus, the usage of OC as a coordinate directly correlates the secondary or consequential material property changes (e.g., density, elongation at break) to the progress of degradation (Celina *et al.*, 2019).

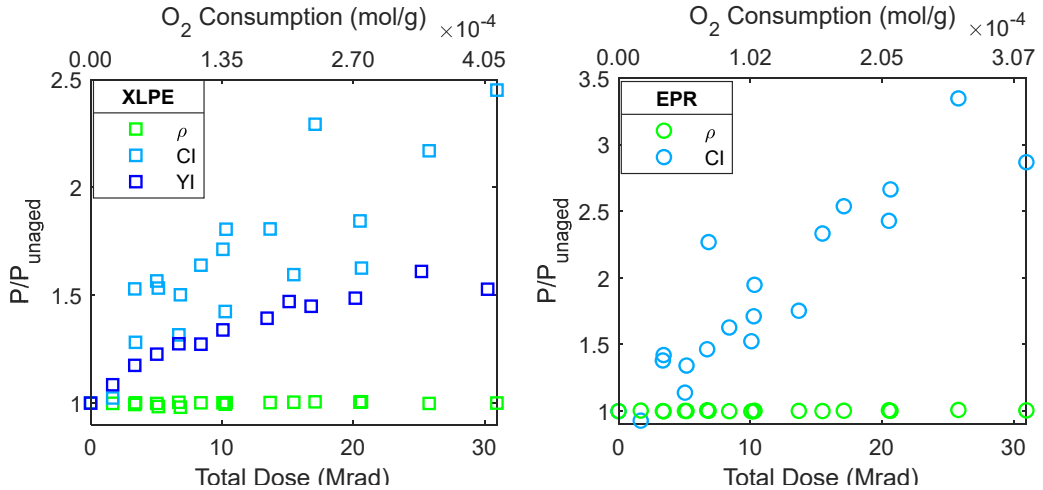

Figure 29. Normalized material properties as a function of total dose and of oxygen consumption for (left) XLPE and (right) EPR.

7. CONCLUSIONS

In this work, nuclear cable insulation samples of the two most common polymer classes, XLPE and EPR, from two of the most sourced manufacturers, RSCC and Okonite, were subjected to gamma irradiation at dose rates of 100, 200, and 300 Gy/hr for up to 42 days at 26°C. The aged samples were used to evaluate oxygen consumption as a sensitive measure of aging for these materials and conditions. For comparison and validation, the aged samples were also characterized using the conventional tests of mass change, density, carbonyl index, and yellowness index.

For both materials, oxygen concentration was found to decrease linearly over time during irradiation for each of the gamma dose rates explored. Mass change, carbonyl index and yellowness index were similarly found to track linearly with radiation at low exposures. Density was not found to be affected by the conditions employed. Yellowness index, a surface sensitive measure, was seen to plateau at higher exposures.

The linearity and hence time equivalency of oxygen consumption rate during oxidative aging was found to enable its use as a viable alternative to time-temperature-superposition as a method for activation energy and lifetime prediction using available literature datasets.

The techniques developed in this work are anticipated to be valuable in the estimation of insulation aging rates under mild conditions approaching service conditions. This is particularly important to correlate laboratory accelerated aging results with cable performance in extended nuclear power plant operation using accelerated conditions that avoid artefacts known to result from too-rapid aging.

8. REFERENCES

Assink, R. A. *et al.* (2005) 'Use of a respirometer to measure oxidation rates of polymeric materials at ambient temperatures', *Polymer*, 46(25), pp. 11648–11654. doi:10.1016/j.polymer.2005.09.069

Assink, R. A., Gillen, K. T., and Bernstein, R. (2005) *Nuclear Energy Plant Optimization (NEPO) final report on aging and condition monitoring of low-voltage cable materials*. SAND2005-7331. Sandia National Laboratories. doi:10.2172/875986.

ASTM D1729-16, A. (2016) 'Standard Practice for Visual Appraisal of Colors and Color Differences of Diffusely-Illuminated Opaque Materials'. West Conshohocken, PA: ASTM International. doi:10.1520/D1729-16.

ASTM D2244-16 (2016) 'Standard Practice for Calculation of Color Tolerances and Color Differences from Instrumentally Measured Color Coordinates'. West Conshohocken, PA: ASTM International. doi:10.1520/D2244-21

ASTM D618-21 (2021) 'Standard Practice for Conditioning Plastics for Testing'. West Conshohocken, PA: ASTM International. doi:10.1520/D0618-21

ASTM D792-20, A. (2020) 'Standard Test Methods for Density and Specific Gravity (Relative Density) of Plastics by Displacement'. West Conshohocken, PA: ASTM International. doi:10.1520/D0792-20

Audouin, L. *et al.* (1994) 'Role of oxygen diffusion in polymer ageing: kinetic and mechanical aspects', *Journal of Materials Science*, 29(3), pp. 569–583. doi:10.1007/BF00445968

Beleites, C. and Sergo, V. (2013) 'hyperSpec: a package to handle hyperspectral data sets in R'. https://github.com/r-hyperspec/hyperSpec.

Bolland, J. L. and Gee, G. (1946) 'Kinetic studies in the chemistry of rubber and related materials. II. The kinetics of oxidation of unconjugated olefins', *Transactions of the Faraday Society.* London, The Society, p. 236. doi: 10.1039/TF9464200236.

Calmet, J. F. *et al.* (2002) 'Irradiation ageing of CSPE/EPR control command electric cables. Correlation between mechanical properties and oxidation', *Radiation Physics and Chemistry*, 63(3–6), pp. 235–239. doi:10.1016/S0969-806X(01)00585-0

Celina, M. *et al.* (1996) 'Anomalous aging phenomena in a crosslinked polyolefin cable insulation', *Radiation Physics and Chemistry*, 48(5), pp. 613–626. doi:10.1016/0969-806X(96)00083-7

Celina, M. *et al.* (2019) 'Overview of accelerated aging and polymer degradation kinetics for combined radiation-thermal environments', *Polymer Degradation and Stability*, 166, pp. 353–378. doi:10.1016/j.polymdegradstab.2019.06.007

Celina, M. C. (2013) 'Review of polymer oxidation and its relationship with materials performance and lifetime prediction', *Polymer Degradation and Stability*, 98(12), pp. 2419–2429. doi: https://doi.org/10.1016/j.polymdegradstab.2013.06.024.

Celina, M. C., Dayile, A. R. and Quintana, A. (2013) 'A perspective on the inherent oxidation sensitivity of epoxy materials', *Polymer*, 54(13), pp. 3290–3296. doi:10.1016/j.polymer.2013.04.042

Celina, M. C., Gillen, K. T. and Lindgren, E. R. (2013) *Nuclear power plant cable materials-review of qualification and currently available aging data for margin assessments in cable performance*, SAND2013-2388. Sandia National Laboratories. doi:10.2172/1096518

Celina, M., Clough, R. L. and Gillen, K. T. (1998) 'Limitations of the Arrhenius Methododolgy', SAND98-1726C, Sandia National Laboratories. https://www.osti.gov/biblio/1535.

Celina, M., Gillen, K. T. and Assink, R. A. (2005) 'Accelerated aging and lifetime prediction: Review of non-Arrhenius behaviour due to two competing processes', *Polymer Degradation and Stability*, 90(3), pp. 395–404. doi:10.1016/j.polymdegradstab.2005.05.004.

Craig, I. H. *et al.* (2005) 'Photo-induced scission and crosslinking in LDPE, LLDPE, and HDPE', *Polymer Engineering & Science*, 45(4), pp. 579–587. doi:10.1002/pen.20313

Da Cruz, M. *et al.* (2016) 'Thermo-oxidative degradation of additive free polyethylene. Part I. Analysis of chemical modifications at molecular and macromolecular scales', *Journal of Applied Polymer Science*, 133(18). doi:10.1002/app.43287

Feller, R. L. *et al.* (2007) 'Photochemical deterioration of poly (vinylbutyral) in the range of wavelengths from middle ultraviolet to the visible', *Polymer Degradation and Stability*, 92(5), pp. 920–931. doi:10.1016/j.polymdegradstab.2005.11.015

Fifield, L. S. *Status Report and Research Plan for Cables Harvested from Crystal River Unit 3 Nuclear Generating Plant*. PNNL-25833. Pacific Northwest National Laboratory. doi:10.2172/1406832.

François-Heude, A. *et al.* (2015) 'A general kinetic model for the photothermal oxidation of polypropylene', *Journal of Photochemistry and Photobiology A: Chemistry*, 296, pp. 48–65. doi: 10.1016/j.jphotochem.2014.08.015

Gillen, K. T. *et al.* (2006) 'Lifetime predictions for semi-crystalline cable insulation materials: I. Mechanical properties and oxygen consumption measurements on EPR materials', *Polymer Degradation and Stability*, 91(9), pp. 2146–2156. doi: https://doi.org/10.1016/j.polymdegradstab.2006.01.009.

Gillen, K. T., Bernstein, R. and Celina, M. (2005) 'Non-Arrhenius behavior for oxidative degradation of chlorosulfonated polyethylene materials', *Polymer Degradation and Stability*, 87(2), pp. 335–346. doi:10.1016/j.polymdegradstab.2004.09.004.

Gillen, K. T., Celina, M. and Bernstein, R. (2003) 'Validation of improved methods for predicting long-term elastomeric seal lifetimes from compression stress–relaxation and oxygen consumption techniques', *Polymer Degradation and Stability*, 82(1), pp. 25–35. doi:10.1016/S0141-3910(03)00159-9

Gillen, K. T., Celina, M. and Clough, R. L. (1999) 'Density measurements as a condition monitoring approach for following the aging of nuclear power plant cable materials', *Radiation Physics and Chemistry*, 56(4), pp. 429–447. doi: 10.1016/S0969-806X(99)00333-3

Gillen, K. T., Celina, M. and Keenan, M. R. (2000) 'Methods for predicting more confident lifetimes of seals in air environments', *Rubber Chemistry and Technology*, 73(2), p. 265. Available at: https://www.proquest.com/docview/220679752?accountid=28112.

Gillen, K. T. and Clough, R. L. (1992) 'Rigorous experimental confirmation of a theoretical model for diffusion-limited oxidation', *Polymer*, 33(20), pp. 4358–4365. doi: 10.1016/0032-3861(92)90280-A

Gillen, K. T., Wise, J. and Clough, R. L. (1995) 'General solution for the basic autoxidation scheme', *Polymer Degradation and Stability*, 47(1), pp. 149–161. doi:10.1016/0141-3910(94)00105-H.

Grebowicz, J., Lau, S. and Wunderlich, B. (1984) 'The thermal properties of polypropylene', in *Journal of Polymer Science: Polymer Symposia*. Wiley Online Library, pp. 19–37. doi:10.1002/polc.5070710106

Martin, J. W. *et al.* (2008) *Service life prediction of polymeric materials: global perspectives*. Springer US. doi: 10.1007/978-0-387-84876-1

Nielsen, A. S., Batchelder, D. N. and Pyrz, R. (2002) 'Estimation of crystallinity of isotactic polypropylene using Raman spectroscopy', *Polymer*, 43(9), pp. 2671–2676. doi:10.1016/S0032-3861(02)00053-8.

NUREG/CR-7153, V. 5 (2014) *Expanded Materials Degradation Assessment (EMDA) Volume 5: Aging*

of Cables and Cable Systems. United State Nuclear Regulatory Commission. https://www.nrc.gov/reading-rm/doc-collections/nuregs/contract/cr7153/v5/index.html

Sarrabi, S. *et al.* (2009) 'Real time analysis of volatile organic compounds from polypropylene thermal oxidation using chemical ionization Fourier transform ion cyclotron resonance mass spectrometry', *Analytical Chemistry*, 81(15), pp. 6013–6020. doi.org/10.1021/ac802353r

Seguchi, T. and Yamamoto, Y. (1986) *Diffusion and solubility of oxygen in γ-ray irradiated polymer insulation materials*. JAERI 1299. Japan Atomic Energy Research Inst. https://inis.iaea.org/collection/NCLCollectionStore/_Public/18/008/18008584.pdf

Subudhi, M. (1996) *Literature review of environmental qualification of safety-related electric cables: Summary of past work Volume 1*. NUREG/CR-6384, BNL-NUREG-52480 Vol.1, Brookhaven National Laboratory for United States Nuclear Regulatory Commission. http://inis.iaea.org/search/search.aspx?orig_q=RN:27059900.

Verdu, J. (2012) *Oxydative ageing of polymers*. John Wiley & Sons. doi:10.1002/9781118562598

Villaran, M. and Lofaro, R. (2009) *Condition Monitoring of Cables Task 3 Report: Condition Monitoring Techniques for Electric Cables*. BNL-90735-2009-IR. Brookhaven National Laboratory. doi:10.2172/1013436.

Wise, J., Gillen, K. T. and Clough, R. L. (1995) 'An ultrasensitive technique for testing the Arrhenius extrapolation assumption for thermally aged elastomers', *Polymer Degradation and Stability*. Barking, Essex : Applied Science Pub, pp. 403–418. doi:10.1016/0141-3910(95)00137-B.

Wise, J., Gillen, K. T. and Clough, R. L. (1997) 'Time development of diffusion-limited oxidation profiles in a radiation environment', *Radiation Physics and Chemistry*, 49(5), pp. 565–573. doi:10.1016/S0969-806X(96)00185-5

Wypych, G. (2020) *Handbook of UV degradation and stabilization*. ChemTec Publishing. doi:10.1016/C2019-0-00344-5

9. APPENDIX

9.1 Gaseous Byproducts

The gaseous byproducts produced during irradiation aging can provide insight into the mechanisms responsible for O_2 consumption and provide valuable information regarding mass uptake of oxygen into the polymer. Amounts of produced gases were calculated similarly to O_2 consumption using gas chromatography described in Section 5.1. Resultant rates of gas production are reported in Table 9. As shown in Figure 30, concentrations of CO_2, CO, CH_4 and H_2 increased linearly with time while the concentration of N_2 and other gases do not appear to have changed significantly over the course of the exposure. It was calculated that 34% and 22% (for XLPE and EPR, respectively) of consumed O_2 became volatile products based on O_2 consumption rates and complimentary CO_2 and CO production rates. Therefore, it was concluded that approximately 66% and 78% (for XLPE and EPR, respectively) of reacted O_2 was incorporated into the polymer structure through oxidation reactions, giving rise to an increase in sample mass.

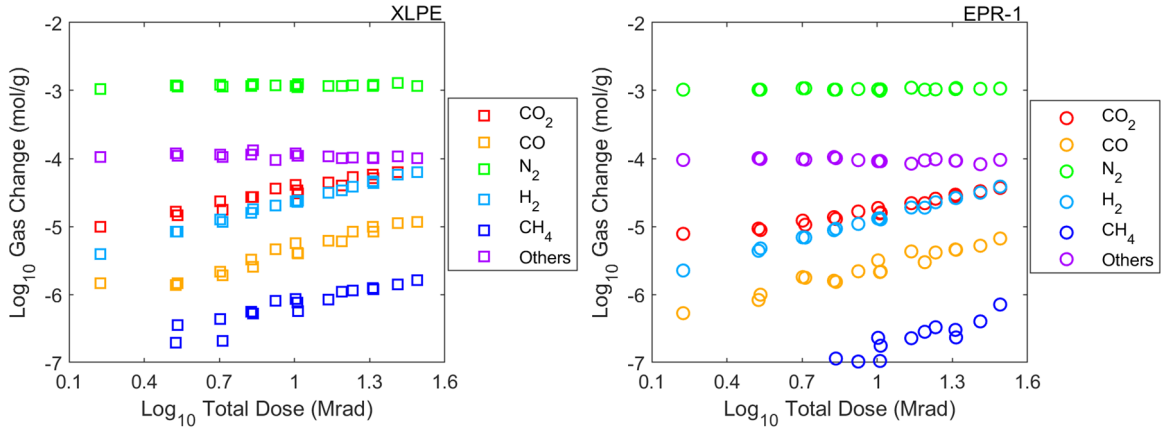

Figure 30. Variation of gas concentration with total dose for (left) XLPE and (right) EPR.

Table 9. Production rates of gas components.

	Gas Production Rates (mol/g/Gy)					Gas Generation/Gas Consumption (g/g)
	Oxygen	Carbon Dioxide	Carbon Monoxide	Methane	Hydrogen	
XLPE	-1.35E-9	2.90E-10	4.44E-11	6.31E-12	2.24E-10	34%
EPR	-1.02E-9	1.41E-10	2.26E-11	1.69E-12	1.27E-10	22%

9.2 Oxygen Consumption Rate Compared to Literature Data

In this section, literature oxygen consumption rates ϕ of polyolefin-based cable materials were compared to those obtained in this work. This was done to (1) further examine in a wider temperature and dose rate ranges whether the basic assumptions behind lifetime prediction are valid, (2) compare different datasets to explore if there is a generic ϕ value for all samples of the same type of polymer, and (3) assess the ϕ results in Section 5.1.

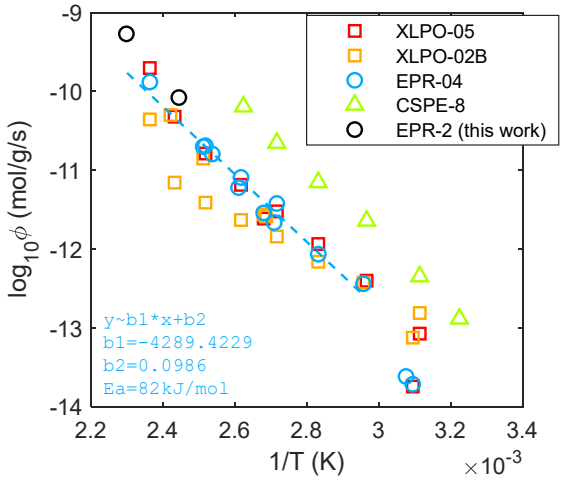

Figure 31. Oxygen consumption rates reported in literature for thermally aged polyolefin samples as a function of reciprocal absolute temperature (Gillen, Celina and Clough, 1999; Gillen, Assink and Bernstein, 2005; Gillen, Bernstein and Celina, 2005; Gillen *et al.*, 2006; Celina, Gillen and Lindgren, 2013).

For the three XLPO and EPR materials investigated in Figure 31, deviation from Arrhenius relation was observed at the lowest temperature (50°C). To determine the temperature dependence near room temperature, preliminary OC experiments of a thermally aged EPR sample (EPR-2) were attempted following the same procedure as described in Section 4.1. Results (not included in this report) were consistent with literature data, as seen in Figure 31, where the linear regression was obtained from OC rates from 65°C to 150°C.

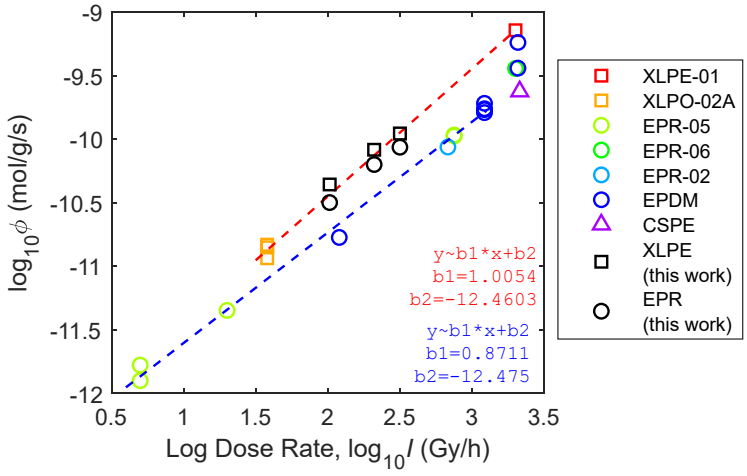

Figure 32. Oxygen consumption rates reported in literature for irradiated polyolefin samples as a function of dose rates (Seguchi and Yamamoto, 1986; Gillen and Clough, 1992; Celina *et al.*, 1996; Gillen, Celina and Clough, 1999; Calmet *et al.*, 2002; Celina, Gillen and Lindgren, 2013).

Literature data of the OC rate of polyolefins during radiation aging below 70°C is shown in Figure 32, where it was assumed irradiation was the predominant stressor of degradation. Deviation from linear dose rate dependence was observed above 1000 Gy/h, where OC vs. total dose curve transitioned to nonlinear, potentially exhibiting a dose rate effect. Empirical linear regression of literature data was also performed for the two materials in Figure 32 to check if our OC rate results reported in Table 7 were comparable to literature data when there was no data obtained at exactly the same aging condition.

Table 10. Oxygen consumption rates reported in Table 7 compared to interpolated literature data.

Material	Dose Rate (Gy/h)	OC rate, ϕ (mol/g/s)	
		Results in Table 7	Interpolated literature data
XLPE	100	4.41E-11	3.55E-11
	200	8.27E-11	7.13E-11
	300	1.11E-10	1.07E-10
EPR	100	3.18E-11	1.85E-11
	200	6.33E-11	3.38E-11
	300	8.67E-11	4.82E-11